BEHAVIOR ROBOT SUITE: Streamlining Real-World Whole-Body Manipulation for Everyday Household Activities

Yunfan Jiang, Ruohan Zhang, Josiah Wong, Chen Wang, Yanjie Ze, Hang Yin, Cem Gokmen,
Shuran Song, Jiajun Wu, Li Fei-Fei
Stanford University

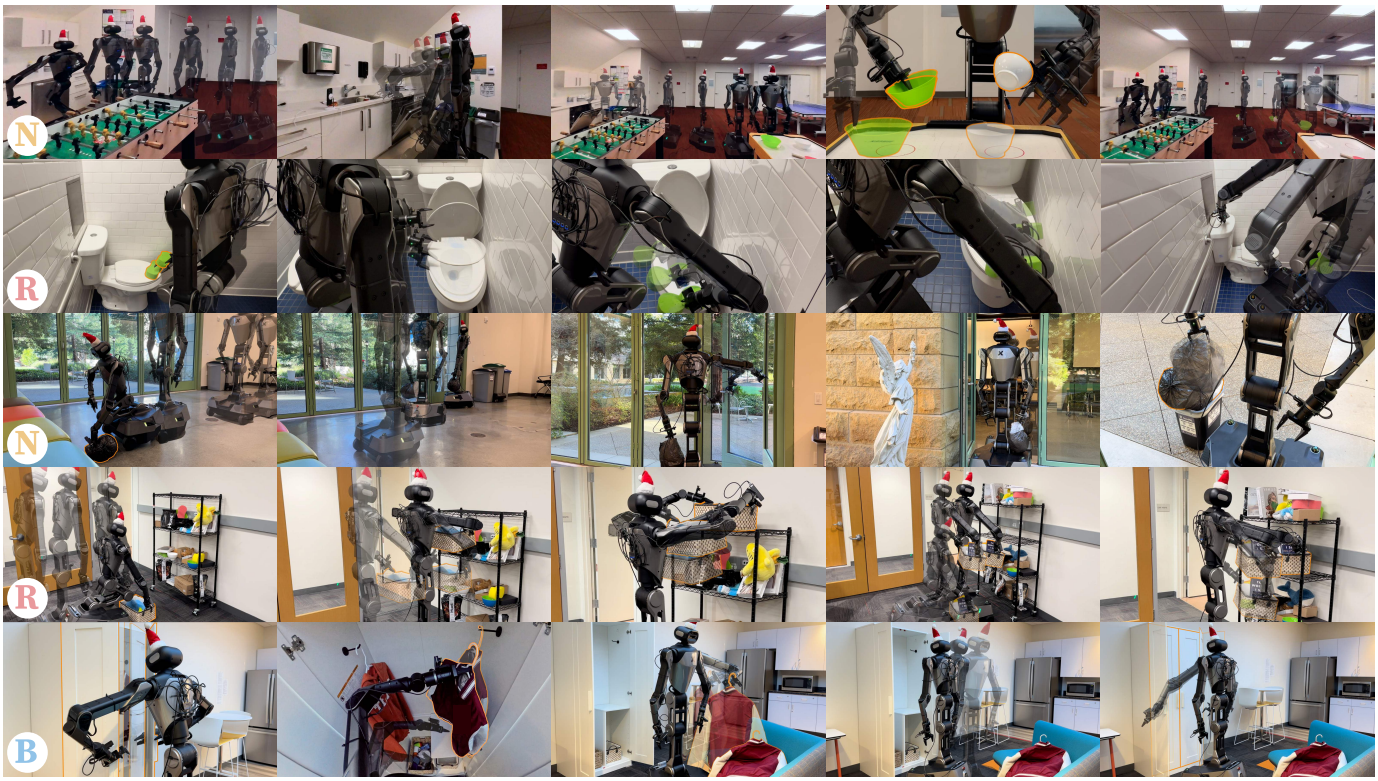

Fig. 1: **Everyday household activities enabled by BEHAVIOR ROBOT SUITE (BRS), showcasing its three core capabilities: bimanual coordination (B), stable and accurate navigation (N), and extensive end-effector reachability (R).** Each row illustrates the rollout trajectory of trained WB-VIMA policies, an imitation learning algorithm we developed, using data collected with JoyLo, our novel whole-body teleoperation interface. While every activity involves multiple capabilities, the most crucial capability for accomplishing each task is highlighted using B, N, and R. Activities from top to bottom are as follows. **1) Clean house after a wild party (N):** The robot navigates to a dishwasher and opens it, then moves to a gaming table to collect bowls. It returns to the dishwasher, places the bowls inside, and closes it. **2) Clean the toilet (R):** The robot picks up a sponge, opens the toilet cover, cleans the seat, then closes the cover and wipes it. Finally, it moves to press the flush button. **3) Take trash outside (N):** The robot navigates to a trash bag in the living room, picks it up, and carries it to a closed door. It opens the door, moves outside, and deposits the trash bag into a trash bin. **4) Put items onto shelves (R):** The robot lifts a box from the ground, moves to a shelf, and places the box on the appropriate level based on available space. **5) Lay clothes out (B):** The robot moves to a wardrobe, opens it, picks up a jacket on a hanger, lays the jacket on a sofa bed, then returns to the wardrobe and closes it.

***Abstract*—Real-world household tasks present significant challenges for mobile manipulation robots. An analysis of existing robotics benchmarks reveals that successful task performance hinges on three key whole-body control capabilities: bimanual coordination, stable and precise navigation, and extensive end-effector reachability. Achieving these capabilities requires careful hardware design, but the resulting system complexity further complicates visuomotor policy learning. To address these**

challenges, we introduce BEHAVIOR ROBOT SUITE (BRS), a comprehensive framework for whole-body manipulation in diverse household tasks. Built on a bimanual, wheeled robot with a 4-DoF torso, BRS integrates a cost-effective whole-body teleoperation interface for data collection and a novel algorithm for learning whole-body visuomotor policies. We evaluate BRS on five challenging household tasks that not only emphasize the three core capabilities but also introduce additional complexities, such as long-range navigation, interaction with articulated and deformable objects, and manipulation in confined spaces. We believe that BRS's integrated robotic embodiment, data collection interface, and learning framework mark a significant step toward enabling real-world whole-body manipulation for everyday household tasks.

I. INTRODUCTION

Developing versatile and capable robots that can assist in everyday life remains a significant challenge in human-centered robotics research [1–4], with a recent emphasis on daily household activities [5–12]. To effectively perform these tasks, robots must navigate extended distances while avoiding obstacles, reach and manipulate objects across different locations and heights, interact with articulated or deformable objects, and execute complex whole-body control. This raises a critical question: *What key capabilities must a robot possess to achieve all these functions?*

To explore this question, we analyze activities from BEHAVIOR-1K [8], a human-centered robotics benchmark comprising 1,000 everyday household activities, defined and prioritized by humans, and instantiated in ecological and virtual environments, including residential houses, offices, and restaurants. Through the analysis, we identify three essential whole-body control capabilities for successfully performing these tasks: **bimanual** coordination, stable and accurate **navigation**, and extensive end-effector **reachability**.

Tasks such as lifting large, heavy objects require **bimanual manipulation** [13, 14], while retrieving tools throughout a house depends on stable and precise **navigation** [15–17]. Complex tasks, such as opening a door while carrying groceries, demand the coordination of both capabilities [18–20]. In addition, everyday objects are distributed across diverse locations and heights, requiring robots to adapt their **reach** accordingly. To illustrate this, we analyze the spatial distribution of task-relevant household objects in BEHAVIOR-1K [8] (Fig. 2). Here, the horizontal distance represents the Euclidean distance from an object to the robot's nearest navigable location, while the vertical distance indicates the object's height from the floor. Notably, the multi-modal distribution of vertical distances highlights the necessity of extensive end-effector reachability, enabling a robot to interact with objects across a wide range of spatial configurations.

But how can a robot effectively achieve these capabilities? Carefully designed robotic hardware that incorporates dual arms, a mobile base, and a flexible torso is essential to enable whole-body manipulation [21]. However, such sophisticated designs introduce significant challenges for policy learning methods, particularly in scaling data collection [22–24] and accurately modeling coordinated whole-body actions in complex

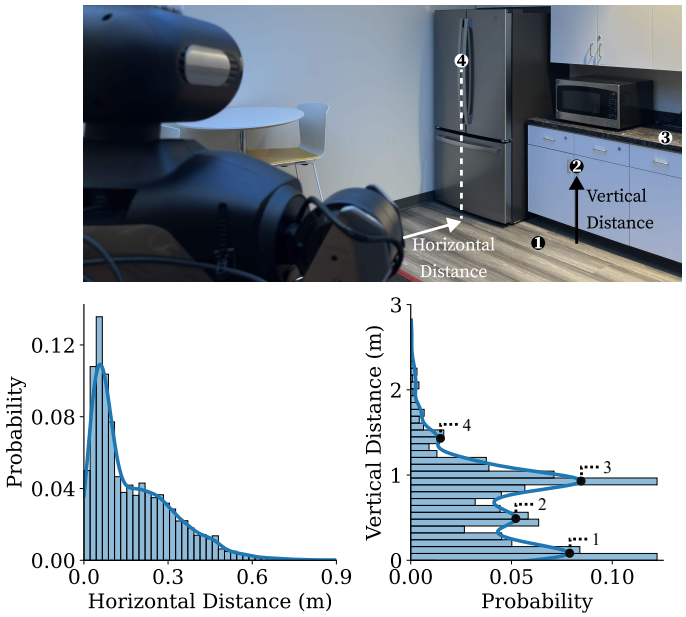

Fig. 2: **Ecological distributions of task-relevant objects involved in daily household activities. Left:** The horizontal distance distribution follows a long-tail distribution. **Right:** The vertical distance distribution exhibits multiple distinct modes, located at $1.43\,\mathrm{m}$, $0.94\,\mathrm{m}$, $0.49\,\mathrm{m}$, and $0.09\,\mathrm{m}$, representing heights at which household objects are typically found.

real-world environments. Current robotic systems often struggle to address these challenges comprehensively [21, 25–31], highlighting the need for more suitable hardware for household tasks, more efficient data collection strategies, and improved models that can capture the hierarchy and interdependencies inherent in whole-body control.

We introduce BEHAVIOR ROBOT SUITE (BRS), a comprehensive framework for learning whole-body manipulation to tackle diverse real-world household tasks (Fig. 1). BRS addresses both hardware and learning challenges through two key innovations. The first is JoyLo, a low-cost, whole-body teleoperation interface designed for general applicability, with a concrete implementation on the Galaxea R1 robot, which is a wheeled dual-arm manipulator with a flexible torso. The second is the Whole-Body VisuoMotor Attention (WB-VIMA) policy, a novel learning algorithm that effectively models coordinated whole-body actions.

JoyLo provides a general, cost-effective approach to whole-body teleoperation by integrating multifunctional joystick controllers mounted on the ends of two 3D-printed arms. The mounting arms serve as scaled-down kinematic twins of the robot's arms, enabling precise bilateral teleoperation [32, 33]. JoyLo also inherits key advantages of puppeteering devices [34–37], including intuitive operation, reduced singularities, and enhanced stability. By grasping the Joy-Con controllers attached to the kinematic-twin arms, users can operate the arms, grippers, torso, and mobile base in unison. This significantly accelerates data collection by allowing users to perform bimanual coordination tasks, navigate safely and

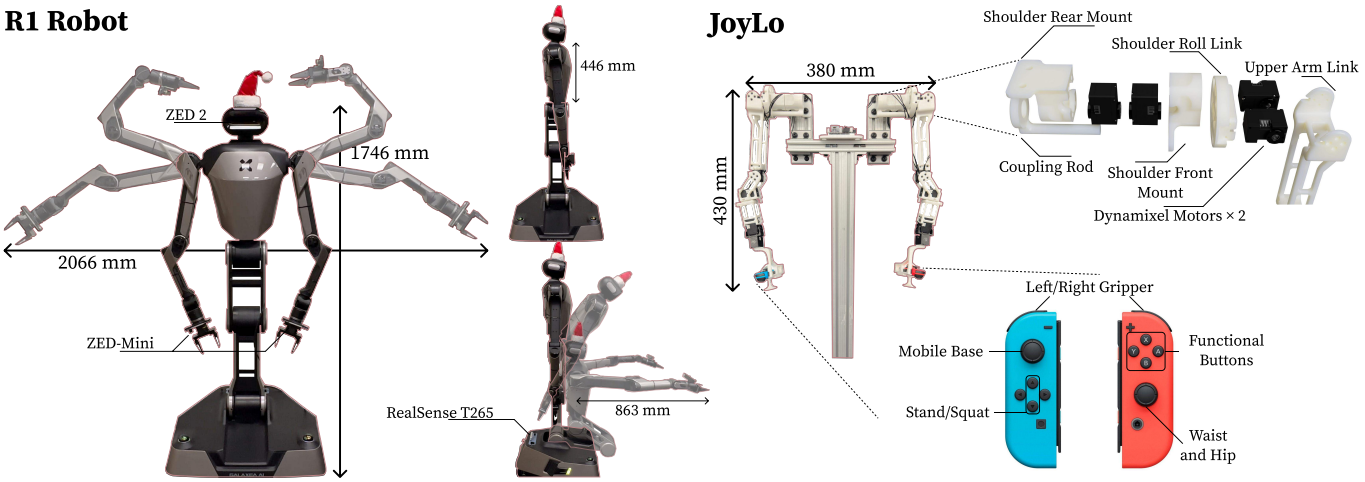

Fig. 3: **BRS hardware system. Left:** The R1 robot's dimensions, range of motion, and onboard sensors. The robot features two 6-DoF arms, each equipped with a parallel jaw gripper, and a 4-DoF torso. The torso is mounted on an omnidirectional mobile base with three wheel motors and three steering motors. **Right:** The JoyLo system, consisting of two kinematic-twin arms constructed using 3D-printed components and low-cost Dynamixel motors. Compact, off-the-shelf Nintendo Joy-Con controllers are mounted at the one end of the arms, serving as the interface for controlling the grippers, torso, and mobile base. To ensure sufficient stall torque for the shoulder joints, two Dynamixel motors are coupled together.

accurately, and guide the end-effectors to effectively reach various locations in 3D space.

WB-VIMA is an imitation learning algorithm designed to model whole-body actions by leveraging the robot's inherent kinematic hierarchy. A key insight behind WB-VIMA is that robot joints exhibit strong interdependencies—small movements in upstream links (e.g., the torso) can lead to large displacements in downstream links (e.g., the end-effectors). To ensure precise coordination across all joints, WB-VIMA conditions action predictions for downstream components on those of upstream components, resulting in more synchronized whole-body movements. Additionally, WB-VIMA dynamically aggregates multi-modal observations using self-attention [38], allowing it to learn expressive policies while mitigating overfitting to proprioceptive inputs.

We evaluate BRS on five representative and challenging real-world household tasks that require the robot to operate in unmodified human living environments. The learned WB-VIMA policies demonstrate strong performance, achieving an average success rate of 58% and a peak success rate of 93%. We believe that BRS 's integrated robotic embodiment, data collection interface, and learning framework mark a significant step toward enabling real-world whole-body manipulation for everyday household tasks.

II. Hardware System

This section introduces the hardware components of BRS. We begin by describing a wheeled dual-arm manipulator with a four-degree-of-freedom (4-DoF) torso, which is suitable for household activities. Next, we present JoyLo, a general framework for building a cost-effective, whole-body teleoperation interface, along with its specific implementation for our robot. An overview of the system is shown in Fig. 3.

A. Robot Platform

We select the Galaxea R1 robot as our platform to meet the three critical capabilities essential for household tasks: **bimanual** coordination, stable and precise **navigation**, and extensive end-effector **reachability**. As illustrated in Fig.3, the R1 robot features two 6-DoF arms mounted on a 4-DoF torso. Each arm is equipped with a parallel jaw gripper and has a maximum payload of $5\,\mathrm{kg}$[1], making it well-suited for manipulating most objects encountered in daily household activities. The torso incorporates four revolute joints: two for waist rotation and hip bending, and two additional joints enabling knee-like motions. This design allows the robot to transition smoothly between standing and squatting positions, enhancing its reachability in household environments. By integrating the torso into the kinematic chain of the end-effectors, the R1 robot achieves an effective reach range from ground level to $2\,\mathrm{m}$ vertically and up to $2.06\,\mathrm{m}$ horizontally, covering the workspace shown in Fig. 2. The arms and torso are controlled using joint impedance controllers, with target joint positions as inputs.

To ensure stable navigation in household environments, the robot's torso is mounted on an omnidirectional mobile base, capable of moving in any direction on the ground plane at a maximum speed of $1.5\,\mathrm{m\,s^{-1}}$. Additionally, the base can independently execute yaw rotations at a maximum angular speed of $3\,\mathrm{rad\,s^{-1}}$. This mobility is powered by three wheel motors and three steering motors. With a $30\,\mathrm{mm}$ ground clearance, the mobile base can traverse most household terrains. It also achieves horizontal accelerations of up to $2.5\,\mathrm{m\,s^{-2}}$, enhancing maneuverability for tasks that require simultaneous movement and manipulation, such as opening doors (Fig. 8). The mobile base is controlled via velocity commands corresponding to its

[1]All numbers related to the robot's hardware capabilities are based on our testing.

three degrees of freedom on the ground plane: forward motion, lateral motion, and yaw rotation.

For perception, we equip the R1 robot with a suite of onboard sensors, including a stereo ZED 2 RGB-D camera as the head camera, two stereo ZED-Mini RGB-D cameras as wrist cameras, and a RealSense T265 tracking camera for visual odometry. All RGB-D cameras operate at $60\,\mathrm{Hz}$, streaming rectified RGB and depth images. The cameras' poses are updated at $500\,\mathrm{Hz}$ via the robot's forward kinematics, enabling the effective fusion of sensory data from all three cameras. This integration supports high-fidelity global and ego-centric 3D perception, such as colored point-cloud observations. Simultaneously, the visual odometry system operates at $200\,\mathrm{Hz}$, providing real-time velocity and acceleration estimates of the mobile base, which is critical feedback for learning precise velocity control for the mobile base.

B. JoyLo: Joy-Con on Low-Cost Kinematic-Twin Arms

To enable seamless control of mobile manipulators with a high number of DoFs and facilitate data collection for downstream policy learning, we introduce JoyLo —a general framework for building a cost-effective whole-body teleoperation interface. As illustrated in Fig. 3, we implement JoyLo on the R1 robot with the following design objectives:

- Efficient whole-body control to coordinate complex movements;
- Rich user feedback for intuitive teleoperation;
- Ensuring high-quality demonstrations for policy learning;
- Low-cost implementation to enhance accessibility;
- A real-time, user-friendly controller for seamless operation.

While our implementation is specific to the R1 robot, the design principles of JoyLo are general and can be adapted to similar robotic platforms.

a) Efficient Whole-Body Control: There exists a wide spectrum of possible approaches for whole-body robot teleoperation, each varying in accuracy, efficiency, applicability, and user experience. At one extreme is kinesthetic teaching, where a human physically guides the robot along target trajectories. While this method is straightforward and accurate [39–42], it is time-consuming and not easily scalable. At the other extreme is motion retargeting, which uses motion-capture devices [25, 43–45] or computer vision techniques [46–52] to directly map human motions to robot executions. While this removes the need for physical interaction, it suffers from embodiment mismatches and limited applicability across different robotic platforms. To strike a balance between intuitiveness, ease of use, and precision for manipulation tasks, we propose a puppeteering-based approach using a pair of kinematic-twin arms with Dynamixel motors as joints. The torso and mobile base movements are controlled via thumbsticks mounted at the ends of the leader arms. Specifically, we utilize off-the-shelf Nintendo Joy-Con controllers due to their compact size, integrated thumbsticks, and multiple functional buttons, which enable rich, customizable functionality. These controllers are attached using a custom-designed enclosure that allows them to slide in and connect rigidly. As illustrated in Fig. 3:

- The left thumbstick issues velocity commands for the mobile base.
- The right thumbstick controls waist rotation and hip bending.
- Two arrow keys adjust torso height for standing and squatting.
- The triggers control the grippers.

With the fully implemented JoyLo system, users can simultaneously control arm movements, gripper operations, upper-body motions, and mobile base navigation, ensuring efficient whole-body control that is accurate, user-friendly, and scalable.

b) Rich User Feedback: Providing sufficient user feedback is essential for improving teleoperation performance. JoyLo achieves this through haptic feedback enabled by bilateral teleoperation [32, 33]. At a high level, the JoyLo arms and the robot arms are kinematically coupled: the JoyLo arms serve as the leader, issuing commands to the robot arms while simultaneously being regularized by the robot's current joint positions. Formally, let $\mathbf{q}_{\text{JoyLo}}$ and $\mathbf{q}_{\text{robot}}$ represent the joint positions of the JoyLo arms and the robot arms, respectively. The torques τ applied to the joints of the JoyLo arms are computed as:

$$\tau = \mathbf{K_p}\left(\mathbf{q}_{\text{robot}} - \mathbf{q}_{\text{JoyLo}}\right) + \mathbf{K_d}\left(\dot{\mathbf{q}}_{\text{robot}} - \dot{\mathbf{q}}_{\text{JoyLo}}\right) - \mathbf{K}, \quad (1)$$

where $\dot{\mathbf{q}}$ denotes joint velocities, $\mathbf{K_p}$ and $\mathbf{K_d}$ are proportional and derivative gain coefficients, and $\mathbf{K}$ represents damping coefficients. Through this formulation, JoyLo provides haptic feedback without requiring additional force sensors [53, 54]. This feedback discourages abrupt user motions and offers proportional resistance when the robot experiences contact. To ensure sufficient stall torque for load-bearing joints in the JoyLo arms, such as the shoulder joints, the two low-cost Dynamixel motors are coupled together, as illustrated in Fig. 3.

c) Optimized for Policy Learning: The choice of teleoperation interface has a significant impact on downstream policy learning performance [55–59], with a key metric being the ability to consistently replay successful trajectories. The replay success rate is crucial because such data are inherently "verified"; that is, imitation learning policies trained on these data only need to replicate the demonstrated actions without compensating for embodiment or kinematic discrepancies. This requires avoiding singularities during data collection, as they can significantly reduce replay success rates. JoyLo ensures these properties by physically constraining the human operator to the robot's embodiment. The kinematic constraints imposed by the kinematic-twin arms prevent the operator from generating infeasible or undeployable actions. Additionally, because the operator directly controls the JoyLo arms at the joint level, singularities are naturally avoided and resolved through intuitive human adjustments, ensuring smooth and reliable demonstrations.

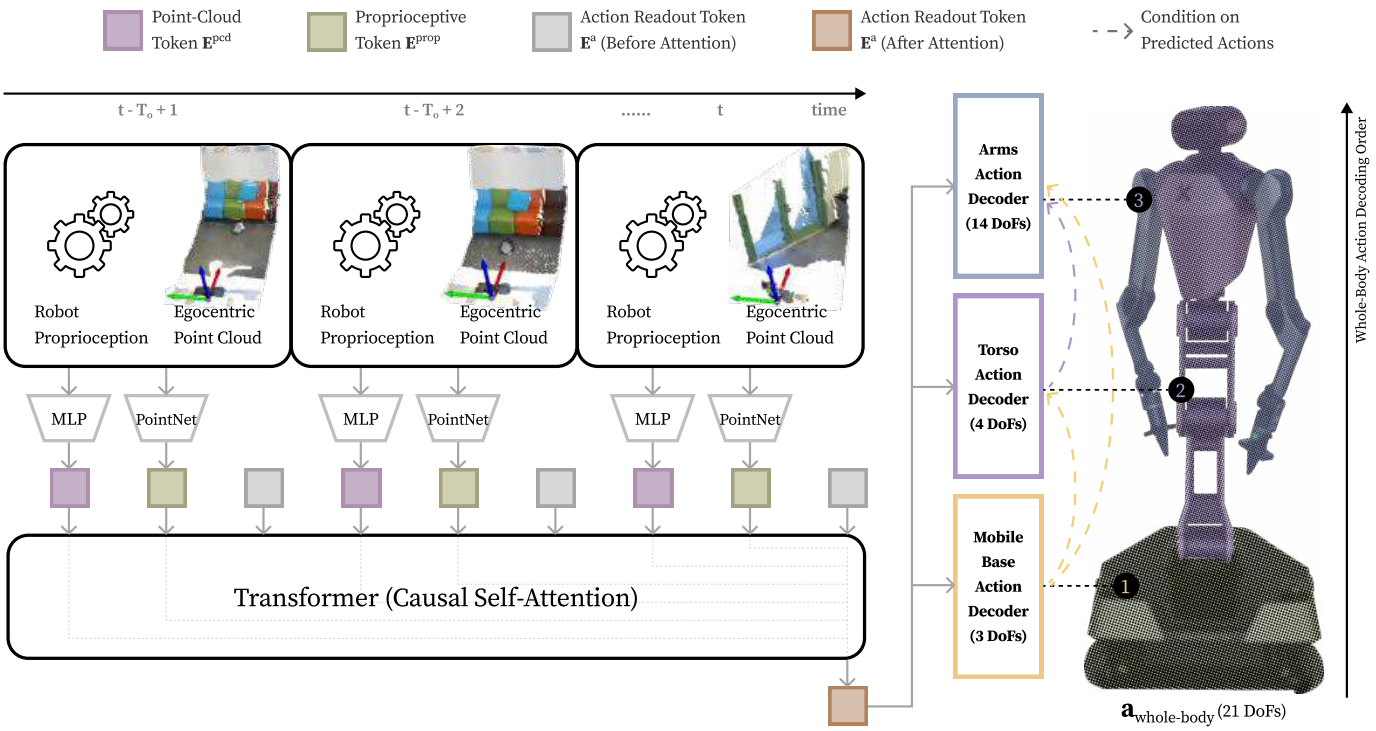

Fig. 4: **WB-VIMA model architecture for imitation learning.** WB-VIMA autoregressively denoises whole-body actions within the embodiment space and dynamically aggregates multi-modal observations using self-attention. By leveraging the hierarchical interdependencies within the robot's embodiment and the rich information provided by multi-modal sensory inputs, WB-VIMA enables effective whole-body policy learning.

d) Low Cost: JoyLo is designed to be highly affordable, with the entire system consisting of 3D-printable arm links, low-cost Dynamixel motors, and off-the-shelf Joy-Con controllers, all totaling under $500. Additionally, its modular design ensures that all components are replaceable, minimizing downtime and eliminating unnecessary repair costs.

e) Easy-to-use real-time controller: To enable efficient operation of JoyLo with the R1 robot, BRS includes an intuitive, real-time controller with Python interfaces. This controller accepts target joint positions for the arms and torso, and target velocities for the mobile base. These inputs are then converted into control commands and transmitted to the robot via Robot Operating System (ROS) topics.

III. Learning Method

This section presents the visuomotor policy learning method introduced in BRS. We begin with a brief preliminary review, followed by an introduction to WB-VIMA, a novel algorithm designed for learning whole-body control policies. WB-VIMA is trained on data collected through JoyLo and is general enough to be applicable to various robot morphologies with multiple articulated components, such as bipedal humanoids. Finally, we detail the training and deployment processes. An overview of the proposed model is illustrated in Fig. 4.

A. Preliminaries

a) Problem Formulation: We formulate robot manipulation as a Markov Decision Process (MDP) $\mathcal{M} := (\mathcal{S}, \mathcal{A}, \mathcal{T}, \rho_0, R)$, where $s \in \mathcal{S}$ represents states, $a \in \mathcal{A}$ represents actions, $\mathcal{T}$ is the transition function, ρ_0 is the initial state distribution, and R is the reward function [60]. A policy π_θ, parameterized by θ, learns the mapping $\mathcal{S} \rightarrow \mathcal{A}$.

b) Denoising Diffusion for Policy Learning: A denoising diffusion probabilistic model (DDPM) [61–63] represents the data distribution $p(x^0)$ as the reverse denoising process of a forward noising process $q(x^k|x^{k-1})$, where Gaussian noise is iteratively applied. Given a noisy sample x^k and timestep k in the forward process, a neural network $\epsilon_\theta(x^k, k)$, parameterized by θ, learns to predict the applied noise ϵ. Starting with a random sample $x^K \sim \mathcal{N}(0, I)$, the reverse denoising process is described as

$$x^{k-1} \sim \mathcal{N}\left(\mu_k\left(x^k, \epsilon_\theta\left(x^k, k\right)\right), \sigma_k^2 I\right), \tag{2}$$

where $\mu_k(\cdot)$ maps the noisy sample x^k and the predicted noise ϵ_θ to the mean of the next distribution, and σ_k^2 is the variance obtained from a predefined schedule for $k = 1, \ldots, K$. Recently, DDPMs have been utilized to model policies π_θ, where the denoising network $\epsilon_\theta(a^k|s, k)$ is trained through behavior cloning [64–66].

B. Whole-Body Visuomotor Attention Policy

We propose WB-VIMA, the **W**hole-**B**ody **Vi**suo**M**otor **A**ttention policy. It is a transformer-based model [38] designed to learn coordinated whole-body actions for mobile manipulation tasks. As illustrated in Fig. 4, WB-VIMA autoregressively denoises whole-body actions across the embodiment space and dynamically aggregates multi-modal observations using self-attention.

a) Autoregressive Whole-Body Action Denoising: In mobile manipulators with multiple articulated components, such as the R1 robot, small errors in the mobile base or torso movements can lead to significant deviations in the end-effectors' poses in Cartesian space. For instance, when the R1 robot is in its neutral pose (Fig. 3) with both arms slightly extended forward, a small $0.17\,\mathrm{rad}$ $(10°)$ movement in the knee joint can result in end-effector displacements of up to $0.14\,\mathrm{m}$. This occurs due to the extended kinematic chain, where errors in upstream joints propagate and amplify in downstream joints. The degree of this amplification varies based on each joint's position within the kinematic tree, making precise coordination essential for accurate whole-body manipulation. To address this issue, we leverage the inherent hierarchy in the robot's embodiment. Specifically, conditioning upper-body action predictions on the predicted actions of the lower body enables the policy to better model coordinated whole-body movements. This approach ensures that downstream joints account for upstream motion, reducing error propagation. The whole-body action decoding process follows an autoregressive structure, where actions are sequentially predicted within the robot's embodiment. At timestep t, the action decoding begins by predicting a future trajectory for the mobile base using the action readout token $\mathbf{E}^a$, encoded from the observations (described in detail later), as the conditioning argument. The predicted trajectory for the mobile base, $\mathbf{a}_{\text{base}} \in \mathbb{R}^{T_a \times 3}$, is then used along with $\mathbf{E}^a$ to predict the future trajectory for the torso, $\mathbf{a}_{\text{torso}} \in \mathbb{R}^{T_a \times 4}$. Finally, $\mathbf{a}_{\text{base}}$, $\mathbf{a}_{\text{torso}}$, and $\mathbf{E}^a$ are used together to predict the future trajectory for the two arms and grippers, $\mathbf{a}_{\text{arms}} \in \mathbb{R}^{T_a \times 14}$. To achieve this, WB-VIMA jointly learns three independent denoising networks for the mobile base, torso, and arms, denoted as ϵ_{base}, ϵ_{torso}, and ϵ_{arms}, respectively. The whole-body actions $\mathbf{a}_{\text{whole-body}} \in \mathbb{R}^{T_a \times 21}$ are sequentially decoded through iterative denoising as follows:

$$
\begin{aligned}
\mathbf{a}_{\text{base}}^{k-1} \sim & \\
& \mathcal{N}\left(\mu_k\left(\mathbf{a}_{\text{base}}^{k}, \epsilon_{\text{base}}\left(\mathbf{a}_{\text{base}}^{k} | \mathbf{E}^a, k\right)\right), \sigma_k^2 I\right), \\
\mathbf{a}_{\text{torso}}^{k-1} \sim & \\
& \mathcal{N}\left(\mu_k\left(\mathbf{a}_{\text{torso}}^{k}, \epsilon_{\text{torso}}\left(\mathbf{a}_{\text{torso}}^{k} | \mathbf{a}_{\text{base}}^{0}, \mathbf{E}^a, k\right)\right), \sigma_k^2 I\right), \\
\mathbf{a}_{\text{arms}}^{k-1} \sim & \\
& \mathcal{N}\left(\mu_k\left(\mathbf{a}_{\text{arms}}^{k}, \epsilon_{\text{arms}}\left(\mathbf{a}_{\text{arms}}^{k} | \mathbf{a}_{\text{torso}}^{0}, \mathbf{a}_{\text{base}}^{0}, \mathbf{E}^a, k\right)\right), \sigma_k^2 I\right).
\end{aligned} \tag{3}
$$

b) Multi-Modal Observation Attention: Observations from multiple modalities are essential to learning autonomous robots that can operate in complex, real-world environments. In WB-VIMA, we use egocentric, colored point clouds as the visual observation and robot joint positions along with mobile base velocities as the proprioceptive observation. The policy must effectively fuse these modalities to make informed predictions while avoiding overfitting to any single source of information. To achieve this, WB-VIMA employs a visuomotor attention network. Concretely, each observation modality is first encoded into an observation token using its respective encoder. In our case, a PointNet [67] encodes point cloud into a point-cloud token, $\mathbf{E}^{\text{pcd}}$, while an MLP encodes proprioception into a proprioceptive token, $\mathbf{E}^{\text{prop}}$. Observation tokens from the current and previous time steps are then assembled to a visuomotor sequence: $\mathbf{S} = [\mathbf{E}^{\text{pcd}}_{t-T_o+1}, \mathbf{E}^{\text{prop}}_{t-T_o+1}, \mathbf{E}^{\text{a}}_{t-T_o+1}, \ldots, \mathbf{E}^{\text{pcd}}_{t}, \mathbf{E}^{\text{prop}}_{t}, \mathbf{E}^{\text{a}}_{t}] \in \mathbb{R}^{3T_o \times E}$, where T_o is the observation window size, E is the token dimension, and $\mathbf{E}^{\text{a}}$ represents the inserted action readout token. The token sequence $\mathbf{S}$ is processed through causal self-attention. Note that action readout tokens only attend to observation tokens that appeared before them in the sequence. Finally, the action readout token corresponding to the last time step, $\mathbf{E}^a_t$, is used for the autoregressive whole-body action decoding discussed above.

c) Efficient Inference: To ensure efficient inference in WB-VIMA for high-frequency closed-loop control, only action readout tokens are used for whole-body action decoding via denoising diffusion. This design enables the use of lightweight UNet-based [68] action heads and a heavier transformer backbone for observation encoding. It strikes a balance between model expressivity and inference latency.

d) Training and Deployment Details: WB-VIMA is trained to predict the added noise from noisy whole-body actions. For each denoising network, the loss is $\mathcal{L} = MSE(\epsilon^k, \epsilon_\theta(\cdot|k))$, where ϵ^k represents the ground-truth added noise and ϵ_θ is the predicted noise. The total loss is the aggregation from all denoising networks. During deployment, inference is performed on the workstation with NVIDIA RTX 4090 GPUs, achieving an effective latency of $0.02\,\mathrm{s}$. We collect data at $10\,\mathrm{Hz}$ while updating inputs to the controllers at $100\,\mathrm{Hz}$. Therefore, a new policy action is issued every $0.1\,\mathrm{s}$ and is repeated 10 times.

IV. Experiments

We conduct experiments to address the following research questions.

- $\mathcal{Q}\mathbf{1}$: What types of household tasks are enabled by BRS?
- $\mathcal{Q}\mathbf{2}$: How does JoyLo compare to other interfaces in terms of data collection efficiency, suitability for policy learning, and user experience?
- $\mathcal{Q}\mathbf{3}$: Does WB-VIMA outperform baseline methods? If so, why do baseline methods fail?
- $\mathcal{Q}\mathbf{4}$: What components contribute to WB-VIMA's effectiveness?
- $\mathcal{Q}\mathbf{5}$: What additional insights can be drawn about the system's overall capabilities?

A. Experiment Settings

Inspired by the everyday activities defined in BEHAVIOR-1K [8], we select five representative household tasks to demonstrate BRS's capabilities (demonstrated in Fig. 1 and detailed in Appendix. D-A). These tasks require the three critical whole-body control capabilities: **bimanual** coordination, stable and accurate **navigation**, and extensive end-effector **reachability**. All tasks are conducted in **real-world**, **unmodified** environments with objects that humans interact with daily. These tasks are long-horizon, ranging from $60\,\mathrm{s}$

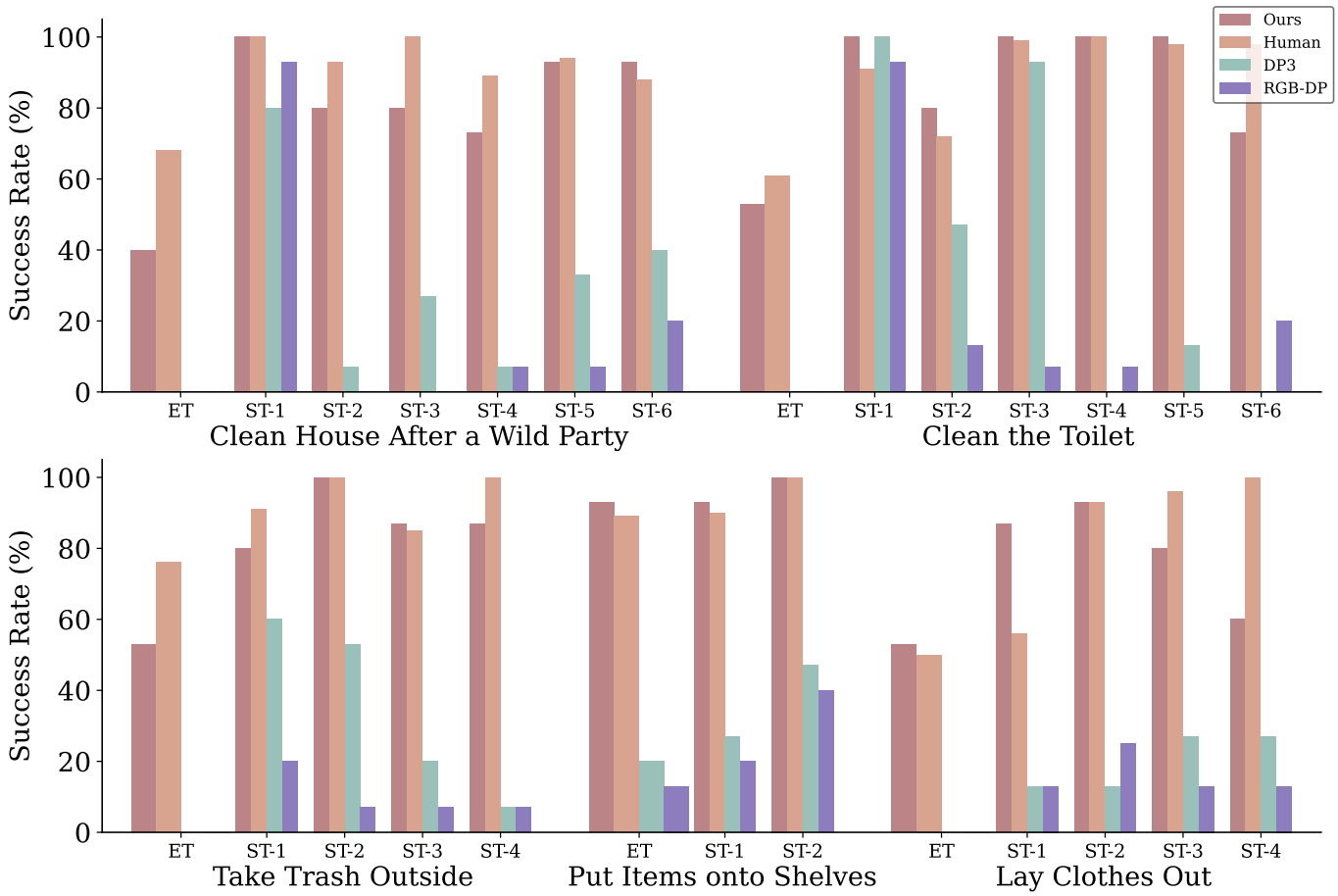

Fig. 5: **Success rate for five representative household activities.** "ET" denotes the entire task and "ST" denotes sub-task. Numerical results are provided in Appendix D-B.

to 210 s for a human operator to complete using JoyLo. Due to the multi-stage nature of these activities, each task is segmented into multiple sub-tasks (**"ST"**). During evaluation, if a sub-task fails, we reset the robot and environment to the initial state of the subsequent sub-task and continue evaluation. Additionally, we report the success rate for the entire task (**"ET"**)—representing the policy's capability to complete the activity end-to-end. For baseline comparisons, we include **DP3** [69] and the RGB image-based diffusion policy (**"RGB-DP"**) [65]. We also report human teleoperation success rate as a reference and track safety violations, defined as robot collisions or motor power losses due to excessive force. Each activity is evaluated 15 times per policy.

B. BRS Enables Various Household Activities (Q1)

As demonstrated by the trained WB-VIMA policy rollouts in Fig. 1, BRS enables the autonomous completion of five complex household tasks in unmodified human environments. Evaluation results in Fig. 5 show that WB-VIMA achieves an average success rate of 58% and a peak success rate of 93% for completing all five tasks end-to-end. A closer analysis of Fig. 5 reveals that WB-VIMA outperforms human teleoperation in certain sub-tasks, particularly those involving contact-rich interactions with articulated objects. Notable examples include opening the toilet cover (ST-2) in "clean the toilet" and opening the wardrobe (ST-1) in "lay clothes out". These sub-tasks are prone to uncoordinated whole-body manipulation, often caused by human errors during teleoperation. In contrast, once trained on successful demonstrations, WB-VIMA learns the precise maneuverability required, predicts coordinated whole-body actions, and reliably accomplishes contact-rich tasks.

TABLE I: **Safety violations during evaluation.** WB-VIMA exhibits minimal collisions with environmental objects and rarely causes motor power loss due to excessive force.

	Clean House After a Wild Party	Clean the Toilet	Take Trash Outside	Put Staff onto Shelves	Lay Clothes Out
WB-VIMA (ours)	**0**	**0**	**1**	**0**	**0**
DP3 [69]	13	**0**	9	**0**	7
RGB-DP [65]	2	2	3	**0**	3

Furthermore, WB-VIMA demonstrates an emergent capability for completing long-horizon, multi-stage tasks. This capability requires strong observation conditioning, allowing WB-VIMA to resolve ambiguous states and estimate task progress accurately. We hypothesize that this capability arises from the synergy between WB-VIMA's multi-modal observation attention and autoregressive whole-body action denoising: the former extracts salient task-relevant features, providing effective conditioning for action denoising; while the latter

generates coherent and coordinated whole-body actions that rarely lead to out-of-distribution states. Additionally, as shown in Table I, WB-VIMA exhibits a near-zero rate of safety violation, such as collisions with environmental fixtures or excessive force applied to robot motors. We attribute this to WB-VIMA's use of colored point-cloud observations, which provide explicit 3D perception of the environment and task semantic information. These observations enable WB-VIMA to generate coordinated whole-body actions that never result in motions with excessive force, inherently respecting safety constraints.

C. JoyLo Is an Efficient, User-Friendly Interface That Provides High-Quality Data for Policy Learning (Q2)

We conducted an extensive user study with 10 participants to evaluate JoyLo's effectiveness and the suitability of its collected data for policy learning. We compare JoyLo against two popular inverse kinematics (IK)-based interfaces: **VR controllers** [25] and **Apple Vision Pro** [70, 71]. The study was conducted in a robotic simulator using the "clean house after a wild party" task to prevent potential damage to the robot or environment. To eliminate bias, participants were exposed to the three interfaces in a randomized order. We measure *success rate* (↑, higher is better) and *completion time* (↓, lower is better) to assess efficiency, and report metrics *replay success rate* (↑) and *singularity ratio* (↓) to assess data quality for policy learning. Here, "success rate" refers to the proportion of successful teleoperation trials, while "replay success rate" measures the success of open-loop execution of collected robot trajectories. This is particularly challenging for long-horizon tasks in stochastic environments. As discussed in Sec. II-B, higher replay success indicates verified data, allowing imitation learning policies to model collected trajectories without accounting for embodiment or kinematic mismatches. We report results for both the entire task and individual subtasks. Participant demographics are shown in Fig. 6b.

As shown in Fig. 6a, JoyLo achieves the highest success rate and shortest completion time among all interfaces. The average success rate for completing the entire task using JoyLo is 5× higher than VR controllers, while no participants complete the entire task using Apple Vision Pro. The median completion time using JoyLo is 23% shorter than with VR controllers. JoyLo particularly excels in articulated object manipulation, such as "open the dishwasher" (ST-2), where it achieves a 67% higher success rate than VR controllers. This is because precise manipulation is crucial for interacting with articulated objects. JoyLo's intuitive operation enables users to generate smooth, highly accurate robot actions, aligning with prior findings that leader-follower arm control improves fine-grained manipulation [37]. Additionally, the most significant sub-task completion time differences between JoyLo and Apple Vision Pro is in "navigate to the dishwasher" (ST-1, 71% faster) and "pick up bowls" (ST-4, 67% faster). Apple Vision Pro's inefficiency stems from its reliance on head movement for mobile base control, making it difficult to coordinate whole-body actions effectively. Since head pose tightly couples with

Fig. 6: **User study results with 10 participants. (a):** JoyLo is the most efficient interface and produces the highest-quality data. "S.R." denotes success rate. "ET Comp. Time" ("ST Comp. Time") refers to entire task (sub-task) completion time. **(b):** Survey results show that JoyLo is unanimously rated as the most user-friendly interface by both robot learning practitioners and novices ("past data collection experience"). Nearly all participants find the Joy-Con helpful for whole-body control ("helpfulness of Joy-Con").

arm and hand tracking, using Apple Vision Pro for mobile manipulation leads to inaccurate tracking and suboptimal teleoperation efficiency, as also reported by Shaw et al. [57].

Furthermore, JoyLo consistently provides the highest-quality data, as indicated by the fact that only data collected with JoyLo successfully replayed in open-loop to complete non-trivial tasks. This is because JoyLo results in the lowest singularity ratio, 78% lower than VR controllers and 85% lower than Apple Vision Pro. The poor data quality in IK-based interfaces stems from suboptimal IK solutions due to the robot's high number of DoFs. While these DoFs improve the workspace coverage and reachability, they also increase the complexity of solving IK, necessitating more sophisticated algorithms. Qualitatively, we observe that using VR controllers or Apple Vision Pro frequently causes self-collisions and jerky

arm motions. In contrast, JoyLo bypasses IK complexity by employing direct joint-to-joint mapping, reducing singularities and ensuring smoother whole-body control. Additionally, the physical constraints of JoyLo's kinematic-twin arms prevent infeasible or undeployable actions, resulting in stable whole-body teleoperation. In terms of user experience, as shown in Fig. 6b, all participants rate JoyLo as the most user-friendly interface. Interestingly, although 70% of participants initially believed IK-based interfaces would be more intuitive, after the study, they unanimously prefer JoyLo. This shift highlights a key difference in data collection for tabletop manipulation and for mobile whole-body manipulation—one common participant complaint is the difficulty of effectively controlling the mobile base and torso using IK-based methods.

D. WB-VIMA Consistently Outperforms Baseline Methods for Household Activities ($\mathcal{Q}\mathbf{3}$)

As shown in Fig. 5, WB-VIMA consistently outperforms the baseline methods DP3 [69] and RGB-DP [65] across all tasks. In terms of end-to-end task success rate, WB-VIMA achieves 13× higher success than DP3 and 21× higher success than RGB-DP. The baseline methods can complete only certain sub-tasks and the relatively simpler "put items onto shelves" task but fail on more complex tasks. For average sub-task performance, WB-VIMA performs 1.6× better than DP3 and 3.4× better than RGB-DP.

The baseline methods fail due to their inability to predict accurate and coordinated whole-body actions. Both DP3 and RGB-DP directly predict flattened 21-DoF actions, ignoring the hierarchical dependencies within the action space. This is problematic because even well-trained policies exhibit modeling errors [72]. If such errors occur in the predicted mobile base or torso actions, they cannot be corrected by arms actions, as all components are predicted simultaneously without interdependency. Whole-body control involves multiple articulated components, meaning inaccurate whole-body actions amplify end-effector drift in the task space, push the robot into out-of-distribution states, and eventually lead to manipulation failures. For instance, DP3 achieves zero success rate when attempting to close the toilet cover (ST-5) in "clean the toilet" because it always moves the base backward without adjusting the torso or arm, preventing the gripper from reaching the cover. In contrast, WB-VIMA conditions torso action denoising on the predicted mobile base actions, and conditions arm action denoising on both torso and base actions. In this way, WB-VIMA can dynamically compensate for inaccuracies in mobile base or torso actions, improving end-effector precision in the task space. Furthermore, since each articulated component conditions its predictions on preceding components in the kinematic tree, WB-VIMA generates more coordinated whole-body actions. Additionally, uncoordinated whole-body actions predicted by baseline methods lead to higher safety violations, as shown in Table I. Examples include colliding with the gaming table when DP3 "cleans house after a wild party", and losing arm power due to excessive force when RGB-DP opens the wardrobe to "lay clothes out".

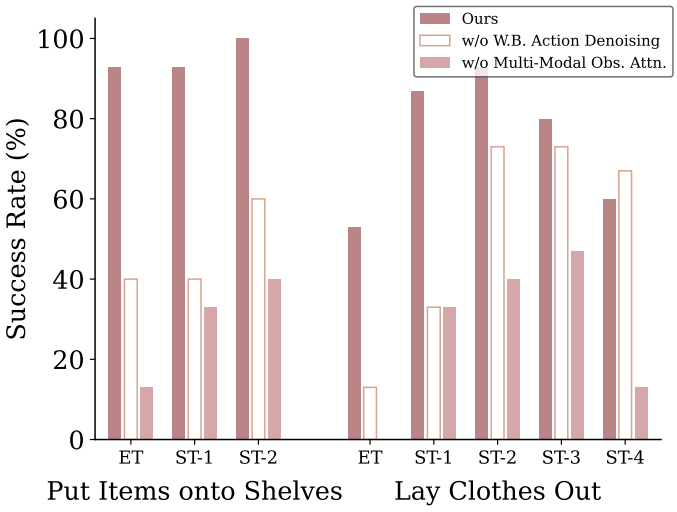

Fig. 7: **Ablation study results for tasks "put items onto shelves" and "lay clothes out".** "w/o W.B. Action Denoising" refers to the variant without autoregressive whole-body action denoising. "w/o Multi-Modal Obs. Attn." refers to the variant without multi-modal observation attention. Numerical results are provided in Appendix D-B.

We also observe that both WB-VIMA and DP3 outperform RGB-DP, highlighting the importance of explicit 3D perception in household tasks and complex environments. Such observations are achieved through fused point clouds from three onboard cameras, providing a unified spatial understanding in the robot frame. In mobile manipulation, accurate base movements are crucial, as the base determines the root position of the robot arms. With explicit 3D perception, policies better learn how to navigate to the proper positions for manipulation. Additionally, compared to DP3, WB-VIMA incorporates task semantic information from colored point clouds, further enhancing salient task-conditioning features through multi-modal observation attention. In contrast, DP3 lacks this capability and often overfits to proprioception—it "stitches" training trajectories based solely on current joint positions while ignoring environmental information.

E. Effects of WB-VIMA's Components on Task Performance ($\mathcal{Q}\mathbf{4}$)

Can models based on explicit 3D perception alone achieve performance comparable to WB-VIMA? The answer is no, as demonstrated by ablation studies on two WB-VIMA variants: one without **autoregressive whole-body action denoising** and the other without **multi-modal observation attention**. As shown in Fig. 7, removing either component significantly degrades overall performance. For the task "put items onto shelves" and the first sub-task "open wardrobe" in "lay clothes out", coordinated whole-body actions are critical for success. Consequently, removing autoregressive whole-body action denoising results in a drastic performance drop of up to 53%. Removing multi-modal observation attention reduces performance across all tasks. In this variant, visual and proprioceptive features are directly concatenated, which potentially

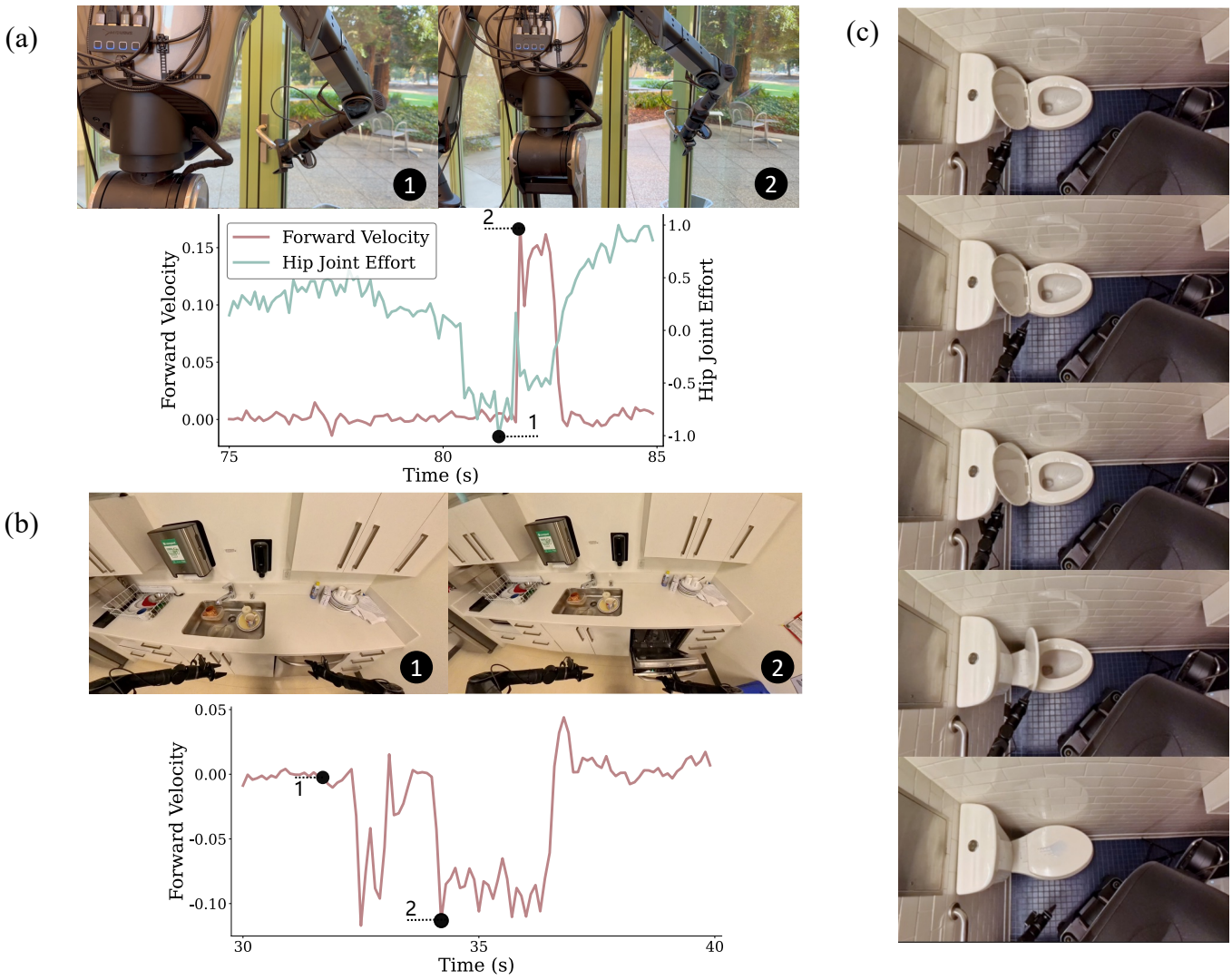

Fig. 8: **Emergent behaviors of learned WB-VIMA policies. (a) and (b):** The trained policies leverage the torso and mobile base to improve maneuverability. In (a), the robot bends its hip forward and advances the mobile base to push the door open. In (b), after grasping the dishwasher handle, the robot moves its base backward to pull the dishwasher open. **(c):** The trained policy exhibits failure recovery behavior. On the first attempt to close the toilet cover, the robot's gripper is too far to reach it. The policy adjusts by tilting the torso forward, bringing the gripper closer, and successfully closing the cover.

creates conflicting representations and reduces the model's expressiveness. As a result, the model tends to ignore visual observations and overfit to proprioception, leading to four environmental collisions due to poor visual awareness.

In summary, the synergy between coherent, coordinated whole-body action predictions and the effective extraction of task-conditioning features from multi-modal observations is essential for WB-VIMA's strong performance in complex, real-world household tasks.

F. Insights into the Capabilities of the Whole System (Q5)

While BRS demonstrates strong performance across diverse household tasks, what additional insights can inform future advances? We highlight two key findings. First, the 4-DoF torso and mobile base greatly enhance the maneuverability that stationary arms do not easily possess. As shown in Figs. 8 a and 8 b, this is evident in tasks involving articulated object interactions where coordinated whole-body movements are necessary, such as "opening the door" (ST-3) in "take trash outside", and "opening the dishwasher" (ST-2) in "clean house after a wild party". To open an unmodified door, the robot learns to bend its torso forward while advancing the mobile base, generating enough inertia to unlock the hinge and push the door open after grasping the handle. Similarly, when opening a dishwasher, the robot moves its base backward, using its entire body to pull the dishwasher door open smoothly. Additionally, we observe that the robot learns to recover from failures. As shown in Fig. 8 c, when the robot fails to close the toilet cover due to limited arm reach, it tilts its torso forward, bringing its arms closer to the toilet. The robot then retries, grasps the toilet cover successfully, and closes the lid smoothly. This emergent behavior highlights the robustness of

the trained WB-VIMA policies.

V. Related Work

Robots for Everyday Household Activities Daily household activities have emerged as a critical scenario and application domain for human-centered robotics research [1–4, 14]. Efforts in this direction can be coarsely classified into two categories: 1) defining household tasks and developing benchmarks [5–12, 73–80], and 2) building robotic systems, usually with learning-based methods, to automate household tasks [21, 30, 31, 57, 81–95]. In the first category, BEHAVIOR-1K [8] defines 1,000 household activities from a large-scale survey. FurnitureBench [9] creates a real-world benchmark for furniture assembly tasks. RoboCasa [12] simulates diverse everyday tasks with AI-generated assets. In the second category, researchers have developed robotic systems that can open doors in real-world environments [31], clean up objects on the ground while following user preferences [86], and cook shrimps [30]. Compared to other types of robots, such as field robots [96–99], rescue robots [100], and surgical robots [101–103], robots for everyday household activities face generalization challenges in the diverse, unstructured, and complex human environments. These challenges can be potentially addressed by learning-based approaches, which rely on both data and learning methods. Unlike previous works that only address one aspect of them, ours is a synergistic framework that consists of both a low-cost, whole-body teleoperation interface for data collection and a general, competent algorithm for whole-body visuomotor policy learning. Additionally, many household activities require **bimanual** coordination and extensive end-effector **reachability**. Previous works rely on a single arm and lifting bodies [26, 77, 89], which limits the household activities that they can effectively perform. In contrast, the hardware system in BRS further unleashes the mobile manipulation capabilities, allowing us to perform more diverse, real-world household activities in complex environments.

Low-Cost Hardware for Robot Learning Recently, developing cost-effective hardware has become a prevalent approach to accelerate the progress of robot learning. These developments include 1) low-cost robots, such as robot arms [37, 104], dexterous hands [105–107], mobile manipulators [21, 30, 31, 81, 93], and humanoids [108–114]; 2) teleoperation interfaces, such as puppeteering devices [35, 37, 57, 115], exoskeletons [56, 58, 116], and AR/VR-based devices [25, 70, 117]; and 3) wearable or portable data collection devices [26, 59, 118–123]. Our development of the JoyLo falls in the second line of research. Compared to other teleoperation interfaces primarily built for stationary arms [35, 56] or mobile manipulators where arms are directly mounted on mobile bases [30, 57], our JoyLo interface enables efficient and user-friendly teleoperation of a dual-arm mobile manipulator with a flexible torso, without the human operator being tethered to the robot [30] or requiring a second user to control the mobile base movement [57]. Additionally, compared to common puppeteering devices [35], JoyLo provides rich haptic feedback through bilateral teleoperation without relying on force sensors [53, 54] or additional real-robot arms [124].

Learning Whole-Body Manipulation Whole-body manipulation refers to the capability of using the entire robot body, including (dual) arms [13, 14, 30, 125, 126], torso [127–130], wheeled or legged base [29, 31, 89, 131–136], and/or other components [137–140], to interact with and manipulate objects. Traditionally, methods to generate whole-body motions rely on motion planning and control [95, 128, 129, 141–145]. Learning-based methods have recently emerged as an effective tool to learn whole-body manipulation policies [27–29, 70, 88, 89, 91, 93, 131–136, 138–140, 146–155]. These works employ reinforcement learning [27, 29, 30, 89, 131, 133–136, 139, 140, 148, 150, 152], behavior cloning [30, 70, 91, 93, 147, 151, 153–155], or rely on large pretrained models [28, 86, 88, 132, 138, 146, 149]. Our proposed WB-VIMA is a novel algorithm for learning whole-body manipulation on a high-DoF, wheeled, dual-arm manipulator with a torso for effectively completing everyday household activities. Unlike previous learning-based methods that either ignore the hierarchical structure of whole-body actions [30, 93, 151], or overlook the interdependencies within the robot embodiment [27, 134, 150], WB-VIMA explicitly models such hierarchy and interdependencies through autoregressive whole-body action denoising, predicting coordinated whole-body actions deployed on a complex robotic system for completing challenging real-world household tasks. Additionally, WB-VIMA dynamically aggregates multi-modal observations through visuomotor self-attention to extract sufficient and salient information for task conditioning, while previous works fail to do so [91, 135, 155].

VI. Limitations and Conclusion

Limitations 1) WB-VIMA is still trained with data collected on the specific R1 robot. It is intriguing to explore how multi-embodiment data and cross-embodiment transfer can benefit the training [22, 94, 156–158]. 2) Our collected data may not be sufficient for scene-level generalization. Future work could explore using large pre-trained models, such as VLA [159–161], to facilitate scene-level generalization capability. 3) It would be complementary to explore how learning whole-body manipulation can benefit from synthetic data [162, 163] or human data [164–166].

This paper presents BRS, a holistic framework for learning whole-body manipulation to tackle diverse real-world household tasks. We identify three core whole-body control capabilities essential for performing household activities: **bimanual** coordination, stable and precise **navigation**, and extensive end-effector **reachability**. Successfully enabling robots to achieve these capabilities with learning-based approaches requires overcoming challenges in both data collection and modeling algorithms. BRS addresses these challenges through two key innovations: 1) JoyLo, a cost-effective whole-body teleoperation interface that enables efficient data collection for learning-based methods; 2) WB-VIMA, a novel algorithm that leverages the robot's embodiment hierarchy and explicitly

models the interdependencies within whole-body actions. The overall BRS system demonstrates strong performance across a range of real-world household tasks, interacting with unmodified objects in natural, unstructured environments. We believe BRS represents a significant step toward enabling robots to perform everyday household tasks with greater autonomy and reliability.

REFERENCES

[1] M. L. Littman, I. Ajunwa, G. Berger, C. Boutilier, M. Currie, F. Doshi-Velez, G. Hadfield, M. C. Horowitz, C. Isbell, H. Kitano, K. Levy, T. Lyons, M. Mitchell, J. Shah, S. Sloman, S. Vallor, and T. Walsh, "Gathering strength, gathering storms: The one hundred year study on artificial intelligence (ai100) 2021 study panel report," *arXiv preprint arXiv: 2210.15767*, 2022.

[2] M. O. Riedl, "Human-centered artificial intelligence and machine learning," *Human Behavior and Emerging Technologies*, vol. 1, no. 1, pp. 33–36, 2019. [Online]. Available: https://onlinelibrary.wiley.com/doi/abs/10.1002/hbe2.117

[3] W. Xu, "Toward human-centered ai: a perspective from human-computer interaction," *Interactions*, vol. 26, no. 4, p. 42–46, Jun. 2019. [Online]. Available: https://doi.org/10.1145/3328485

[4] B. Shneiderman, "Bridging the gap between ethics and practice: Guidelines for reliable, safe, and trustworthy human-centered ai systems," *ACM Trans. Interact. Intell. Syst.*, vol. 10, no. 4, Oct. 2020. [Online]. Available: https://doi.org/10.1145/3419764

[5] D. Batra, A. X. Chang, S. Chernova, A. J. Davison, J. Deng, V. Koltun, S. Levine, J. Malik, I. Mordatch, R. Mottaghi, M. Savva, and H. Su, "Rearrangement: A challenge for embodied ai," *arXiv preprint arXiv: 2011.01975*, 2020.

[6] S. Srivastava, C. Li, M. Lingelbach, R. Martín-Martín, F. Xia, K. E. Vainio, Z. Lian, C. Gokmen, S. Buch, C. K. Liu, S. Savarese, H. Gweon, J. Wu, and L. Fei-Fei, "BEHAVIOR: benchmark for everyday household activities in virtual, interactive, and ecological environments," in *Conference on Robot Learning, 8-11 November 2021, London, UK*, ser. Proceedings of Machine Learning Research, A. Faust, D. Hsu, and G. Neumann, Eds., vol. 164. PMLR, 2021, pp. 477–490. [Online]. Available: https://proceedings.mlr.press/v164/srivastava22a.html

[7] A. Szot, A. Clegg, E. Undersander, E. Wijmans, Y. Zhao, J. Turner, N. Maestre, M. Mukadam, D. S. Chaplot, O. Maksymets, A. Gokaslan, V. Vondruš, S. Dharur, F. Meier, W. Galuba, A. Chang, Z. Kira, V. Koltun, J. Malik, M. Savva, and D. Batra, "Habitat 2.0: Training home assistants to rearrange their habitat," in *Advances in Neural Information Processing Systems*, M. Ranzato, A. Beygelzimer, Y. Dauphin, P. Liang, and J. W. Vaughan, Eds., vol. 34. Curran Associates, Inc., 2021, pp. 251–266. [Online]. Available: https://proceedings.neurips.cc/paper_files/paper/2021/file/021bbc7ee20b71134d53e20206bd6feb-Paper.pdf

[8] C. Li, C. Gokmen, G. Levine, R. Martín-Martín, S. Srivastava, C. Wang, J. Wong, R. Zhang, M. Lingelbach, J. Sun, M. Anvari, M. Hwang, M. Sharma, A. Aydin, D. Bansal, S. Hunter, K.-Y. Kim, A. Lou, C. R. Matthews, I. Villa-Renteria, J. H. Tang, C. Tang, F. Xia, S. Savarese, H. Gweon, K. Liu, J. Wu, and L. Fei-Fei, "BEHAVIOR-1k: A benchmark for embodied AI with 1,000 everyday activities and realistic simulation," in *6th Annual Conference on Robot Learning*, 2022. [Online]. Available: https://openreview.net/forum?id=_8DoIe8G3t

[9] M. Heo, Y. Lee, D. Lee, and J. J. Lim, "Furniturebench: Reproducible real-world benchmark for long-horizon complex manipulation," in *Robotics: Science and Systems XIX, Daegu, Republic of Korea, July 10-14, 2023*, K. E. Bekris, K. Hauser, S. L. Herbert, and J. Yu, Eds., 2023. [Online]. Available: https://doi.org/10.15607/RSS.2023.XIX.041

[10] S. Yenamandra, A. Ramachandran, K. Yadav, A. S. Wang, M. Khanna, T. Gervet, T.-Y. Yang, V. Jain, A. Clegg, J. M. Turner, Z. Kira, M. Savva, A. X. Chang, D. S. Chaplot, D. Batra, R. Mottaghi, Y. Bisk, and C. Paxton, "Homerobot: Open-vocabulary mobile manipulation," in *7th Annual Conference on Robot Learning*, 2023. [Online]. Available: https://openreview.net/forum?id=b-cto-fetlz

[11] A. Shukla, S. Tao, and H. Su, "Maniskill-hab: A benchmark for low-level manipulation in home rearrangement tasks," *arXiv preprint arXiv: 2412.13211*, 2024.

[12] S. Nasiriany, A. Maddukuri, L. Zhang, A. Parikh, A. Lo, A. Joshi, A. Mandlekar, and Y. Zhu, "Robocasa: Large-scale simulation of everyday tasks for generalist robots," *arXiv preprint arXiv: 2406.02523*, 2024.

[13] C. Smith, Y. Karayiannidis, L. Nalpantidis, X. Gratal, P. Qi, D. V. Dimarogonas, and D. Kragic, "Dual arm manipulation—a survey," *Robotics and Autonomous Systems*, vol. 60, no. 10, pp. 1340–1353, 2012. [Online]. Available: https://www.sciencedirect.com/science/article/pii/S092188901200108X

[14] A. Billard and D. Kragic, "Trends and challenges in robot manipulation," *Science*, vol. 364, no. 6446, p. eaat8414, 2019. [Online]. Available: https://www.science.org/doi/abs/10.1126/science.aat8414

[15] G. Desouza and A. Kak, "Vision for mobile robot navigation: a survey," *IEEE Transactions on Pattern Analysis and Machine Intelligence*, vol. 24, no. 2, pp. 237–267, 2002.

[16] T. Kruse, A. K. Pandey, R. Alami, and A. Kirsch, "Human-aware robot navigation: A survey," *Robotics and Autonomous Systems*, vol. 61, no. 12, pp. 1726–1743, 2013. [Online]. Available: https://www.sciencedirect.com/science/article/pii/S0921889013001048

[17] X. Xiao, B. Liu, G. Warnell, and P. Stone,

"Motion planning and control for mobile robot navigation using machine learning: a survey," *Autonomous Robots*, vol. 46, pp. 569–597, 2022. [Online]. Available: https://link.springer.com/article/10.1007/s10514-022-10039-8/fulltext.html

[18] L. Peterson, D. Austin, and D. Kragic, "High-level control of a mobile manipulator for door opening," in *Proceedings. 2000 IEEE/RSJ International Conference on Intelligent Robots and Systems (IROS 2000) (Cat. No.00CH37113)*, vol. 3, 2000, pp. 2333–2338 vol.3.

[19] N. Banerjee, X. Long, R. Du, F. Polido, S. Feng, C. G. Atkeson, M. Gennert, and T. Padir, "Human-supervised control of the atlas humanoid robot for traversing doors," in *2015 IEEE-RAS 15th International Conference on Humanoid Robots (Humanoids)*, 2015, pp. 722–729.

[20] M. DeDonato, F. Polido, K. Knoedler, B. P. W. Babu, N. Banerjee, C. P. Bove, X. Cui, R. Du, P. Franklin, J. P. Graff, P. He, A. Jaeger, L. Li, D. Berenson, M. A. Gennert, S. Feng, C. Liu, X. Xinjilefu, J. Kim, C. G. Atkeson, X. Long, and T. Padır, "Team wpi-cmu: Achieving reliable humanoid behavior in the darpa robotics challenge," *Journal of Field Robotics*, vol. 34, no. 2, pp. 381–399, 2017. [Online]. Available: https://onlinelibrary.wiley.com/doi/abs/10.1002/rob.21685

[21] M. Bajracharya, J. Borders, R. Cheng, D. Helmick, L. Kaul, D. Kruse, J. Leichty, J. Ma, C. Matl, F. Michel, C. Papazov, J. Petersen, K. Shankar, and M. Tjersland, "Demonstrating mobile manipulation in the wild: A metrics-driven approach," *Robotics: Science and Systems*, 2023. [Online]. Available: https://arxiv.org/abs/2401.01474v1

[22] A. O'Neill, A. Rehman, A. Maddukuri, A. Gupta, A. Padalkar, A. Lee, A. Pooley, A. Gupta, A. Mandlekar, A. Jain, A. Tung, A. Bewley, A. Herzog, A. Irpan, A. Khazatsky, A. Rai, A. Gupta, A. Wang, A. Singh, A. Garg, A. Kembhavi, A. Xie, A. Brohan, A. Raffin, A. Sharma, A. Yavary, A. Jain, A. Balakrishna, A. Wahid, B. Burgess-Limerick, B. Kim, B. Schölkopf, B. Wulfe, B. Ichter, C. Lu, C. Xu, C. Le, C. Finn, C. Wang, C. Xu, C. Chi, C. Huang, C. Chan, C. Agia, C. Pan, C. Fu, C. Devin, D. Xu, D. Morton, D. Driess, D. Chen, D. Pathak, D. Shah, D. Büchler, D. Jayaraman, D. Kalashnikov, D. Sadigh, E. Johns, E. Foster, F. Liu, F. Ceola, F. Xia, F. Zhao, F. Stulp, G. Zhou, G. S. Sukhatme, G. Salhotra, G. Yan, G. Feng, G. Schiavi, G. Berseth, G. Kahn, G. Wang, H. Su, H.-S. Fang, H. Shi, H. Bao, H. Ben Amor, H. I. Christensen, H. Furuta, H. Walke, H. Fang, H. Ha, I. Mordatch, I. Radosavovic, I. Leal, J. Liang, J. Abou-Chakra, J. Kim, J. Drake, J. Peters, J. Schneider, J. Hsu, J. Bohg, J. Bingham, J. Wu, J. Gao, J. Hu, J. Wu, J. Wu, J. Sun, J. Luo, J. Gu, J. Tan, J. Oh, J. Wu, J. Lu, J. Yang, J. Malik, J. Silvério, J. Hejna, J. Booher, J. Tompson, J. Yang, J. Salvador, J. J. Lim, J. Han, K. Wang, K. Rao, K. Pertsch, K. Hausman, K. Go, K. Gopalakrishnan, K. Goldberg, K. Byrne, K. Oslund, K. Kawaharazuka, K. Black, K. Lin, K. Zhang, K. Ehsani, K. Lekkala, K. Ellis, K. Rana, K. Srinivasan, K. Fang, K. P. Singh, K.-H. Zeng, K. Hatch, K. Hsu, L. Itti, L. Y. Chen, L. Pinto, L. Fei-Fei, L. Tan, L. J. Fan, L. Ott, L. Lee, L. Weihs, M. Chen, M. Lepert, M. Memmel, M. Tomizuka, M. Itkina, M. G. Castro, M. Spero, M. Du, M. Ahn, M. C. Yip, M. Zhang, M. Ding, M. Heo, M. K. Srirama, M. Sharma, M. J. Kim, N. Kanazawa, N. Hansen, N. Heess, N. J. Joshi, N. Suenderhauf, N. Liu, N. Di Palo, N. M. M. Shafiullah, O. Mees, O. Kroemer, O. Bastani, P. R. Sanketi, P. T. Miller, P. Yin, P. Wohlhart, P. Xu, P. D. Fagan, P. Mitrano, P. Sermanet, P. Abbeel, P. Sundaresan, Q. Chen, Q. Vuong, R. Rafailov, R. Tian, R. Doshi, R. Martín-Martín, R. Baijal, R. Scalise, R. Hendrix, R. Lin, R. Qian, R. Zhang, R. Mendonca, R. Shah, R. Hoque, R. Julian, S. Bustamante, S. Kirmani, S. Levine, S. Lin, S. Moore, S. Bahl, S. Dass, S. Sonawani, S. Song, S. Xu, S. Haldar, S. Karamcheti, S. Adebola, S. Guist, S. Nasiriany, S. Schaal, S. Welker, S. Tian, S. Ramamoorthy, S. Dasari, S. Belkhale, S. Park, S. Nair, S. Mirchandani, T. Osa, T. Gupta, T. Harada, T. Matsushima, T. Xiao, T. Kollar, T. Yu, T. Ding, T. Davchev, T. Z. Zhao, T. Armstrong, T. Darrell, T. Chung, V. Jain, V. Vanhoucke, W. Zhan, W. Zhou, W. Burgard, X. Chen, X. Wang, X. Zhu, X. Geng, X. Liu, X. Liangwei, X. Li, Y. Lu, Y. J. Ma, Y. Kim, Y. Chebotar, Y. Zhou, Y. Zhu, Y. Wu, Y. Xu, Y. Wang, Y. Bisk, Y. Cho, Y. Lee, Y. Cui, Y. Cao, Y.-H. Wu, Y. Tang, Y. Zhu, Y. Zhang, Y. Jiang, Y. Li, Y. Li, Y. Iwasawa, Y. Matsuo, Z. Ma, Z. Xu, Z. J. Cui, Z. Zhang, and Z. Lin, "Open x-embodiment: Robotic learning datasets and rt-x models : Open x-embodiment collaboration0," in *2024 IEEE International Conference on Robotics and Automation (ICRA)*, 2024, pp. 6892–6903.

[23] H. Walke, K. Black, A. Lee, M. J. Kim, M. Du, C. Zheng, T. Zhao, P. Hansen-Estruch, Q. Vuong, A. W. He, V. Myers, K. Fang, C. Finn, and S. Levine, "Bridgedata v2: A dataset for robot learning at scale," *Conference on Robot Learning*, 2023.

[24] A. Khazatsky, K. Pertsch, S. Nair, A. Balakrishna, S. Dasari, S. Karamcheti, S. Nasiriany, M. K. Srirama, L. Y. Chen, K. Ellis, P. D. Fagan, J. Hejna, M. Itkina, M. Lepert, Y. J. Ma, P. T. Miller, J. Wu, S. Belkhale, S. Dass, H. Ha, A. Jain, A. Lee, Y. Lee, M. Memmel, S. Park, I. Radosavovic, K. Wang, A. Zhan, K. Black, C. Chi, K. B. Hatch, S. Lin, J. Lu, J. Mercat, A. Rehman, P. R. Sanketi, A. Sharma, C. Simpson, Q. Vuong, H. R. Walke, B. Wulfe, T. Xiao, J. H. Yang, A. Yavary, T. Z. Zhao, C. Agia, R. Baijal, M. G. Castro, D. Chen, Q. Chen, T. Chung, J. Drake, E. P. Foster, J. Gao, D. A. Herrera, M. Heo, K. Hsu, J. Hu, D. Jackson, C. Le, Y. Li, K. Lin, R. Lin, Z. Ma, A. Maddukuri, S. Mirchandani, D. Morton, T. Nguyen, A. O'Neill,

R. Scalise, D. Seale, V. Son, S. Tian, E. Tran, A. E. Wang, Y. Wu, A. Xie, J. Yang, P. Yin, Y. Zhang, O. Bastani, G. Berseth, J. Bohg, K. Goldberg, A. Gupta, A. Gupta, D. Jayaraman, J. J. Lim, J. Malik, R. Martín-Martín, S. Ramamoorthy, D. Sadigh, S. Song, J. Wu, M. C. Yip, Y. Zhu, T. Kollar, S. Levine, and C. Finn, "Droid: A large-scale in-the-wild robot manipulation dataset," *Robotics: Science and Systems*, 2024.

[25] S. Dass, W. Ai, Y. Jiang, S. Singh, J. Hu, R. Zhang, P. Stone, B. Abbatematteo, and R. Martín-Martín, "Telemoma: A modular and versatile teleoperation system for mobile manipulation," *arXiv preprint arXiv: 2403.07869*, 2024.

[26] N. M. M. Shafiullah, A. Rai, H. Etukuru, Y. Liu, I. Misra, S. Chintala, and L. Pinto, "On bringing robots home," *arXiv preprint arXiv: 2311.16098*, 2023. [Online]. Available: https://arxiv.org/abs/2311.16098v1

[27] J. Hu, P. Stone, and R. Mart'in-Mart'in, "Causal policy gradient for whole-body mobile manipulation," *Robotics: Science and Systems*, 2023. [Online]. Available: https://arxiv.org/abs/2305.04866v4

[28] Z. Jiang, Y. Xie, J. Li, Y. Yuan, Y. Zhu, and Y. Zhu, "Harmon: Whole-body motion generation of humanoid robots from language descriptions," in *8th Annual Conference on Robot Learning*, 2024. [Online]. Available: https://openreview.net/forum?id=UUZ4Yw3lt0

[29] S. Uppal, A. Agarwal, H. Xiong, K. Shaw, and D. Pathak, "Spin: Simultaneous perception, interaction and navigation," *Computer Vision and Pattern Recognition*, 2024. [Online]. Available: https://arxiv.org/abs/2405.07991v1

[30] Z. Fu, T. Z. Zhao, and C. Finn, "Mobile aloha: Learning bimanual mobile manipulation with low-cost whole-body teleoperation," *arXiv preprint arXiv: 2401.02117*, 2024. [Online]. Available: https://arxiv.org/abs/2401.02117v1

[31] H. Xiong, R. Mendonca, K. Shaw, and D. Pathak, "Adaptive mobile manipulation for articulated objects in the open world," *arXiv preprint arXiv: 2401.14403*, 2024.

[32] B. Hannaford, "A design framework for teleoperators with kinesthetic feedback," *IEEE Transactions on Robotics and Automation*, vol. 5, no. 4, pp. 426–434, 1989.

[33] D. Lawrence, "Stability and transparency in bilateral teleoperation," *IEEE Transactions on Robotics and Automation*, vol. 9, no. 5, pp. 624–637, 1993.

[34] T. Hulin, K. Hertkorn, P. Kremer, S. Schätzle, J. Artigas, M. Sagardia, F. Zacharias, and C. Preusche, "The dlr bimanual haptic device with optimized workspace," in *2011 IEEE International Conference on Robotics and Automation*, 2011, pp. 3441–3442.

[35] P. Wu, Y. Shentu, Z. Yi, X. Lin, and P. Abbeel, "Gello: A general, low-cost, and intuitive teleoperation framework for robot manipulators," *IEEE/RJS International Conference on Intelligent RObots and Systems*, 2023.

[36] A. Purushottam, C. Xu, Y. Jung, and J. Ramos, "Dynamic mobile manipulation via whole-body bilateral teleoperation of a wheeled humanoid," *IEEE Robotics and Automation Letters*, vol. 9, no. 2, pp. 1214–1221, 2024.

[37] T. Z. Zhao, V. Kumar, S. Levine, and C. Finn, "Learning fine-grained bimanual manipulation with low-cost hardware," *arXiv preprint arXiv: 2304.13705*, 2023. [Online]. Available: https://arxiv.org/abs/2304.13705v1

[38] A. Vaswani, N. M. Shazeer, N. Parmar, J. Uszkoreit, L. Jones, A. N. Gomez, L. Kaiser, and I. Polosukhin, "Attention is all you need," *Neural Information Processing Systems*, 2017. [Online]. Available: https://arxiv.org/abs/1706.03762v7

[39] S. C. Petar Kormushev and D. G. Caldwell, "Imitation learning of positional and force skills demonstrated via kinesthetic teaching and haptic input," *Advanced Robotics*, vol. 25, no. 5, pp. 581–603, 2011. [Online]. Available: https://doi.org/10.1163/016918611X558261

[40] H. Ravichandar, A. S. Polydoros, S. Chernova, and A. Billard, "Recent advances in robot learning from demonstration," *Annual Review of Control, Robotics, and Autonomous Systems*, vol. 3, no. Volume 3, 2020, pp. 297–330, 2020. [Online]. Available: https://www.annualreviews.org/content/journals/10.1146/annurev-control-100819-063206

[41] S. Wrede, C. Emmerich, R. Grünberg, A. Nordmann, A. Swadzba, and J. Steil, "A user study on kinesthetic teaching of redundant robots in task and configuration space," *J. Hum.-Robot Interact.*, vol. 2, no. 1, p. 56–81, Feb. 2013. [Online]. Available: https://doi.org/10.5898/JHRI.2.1.Wrede

[42] M. Hagenow, D. Kontogiorgos, Y. Wang, and J. Shah, "Versatile demonstration interface: Toward more flexible robot demonstration collection," *arXiv preprint arXiv: 2410.19141*, 2024. [Online]. Available: https://arxiv.org/abs/2410.19141v1

[43] A. Setapen, M. Quinlan, and P. Stone, "Marionet: motion acquisition for robots through iterative online evaluative training," in *Proceedings of the 9th International Conference on Autonomous Agents and Multiagent Systems: Volume 1 - Volume 1*, ser. AAMAS '10. Richland, SC: International Foundation for Autonomous Agents and Multiagent Systems, 2010, p. 1435–1436.

[44] C. Stanton, A. Bogdanovych, and E. Ratanasena, "Teleoperation of a humanoid robot using full-body motion capture, example movements, and machine learning," in *Australasian Conference on Robotics and Automation, ACRA*, 12 2012.

[45] M. Arduengo, A. Arduengo, A. Colomé, J. Lobo-Prat, and C. Torras, "Human to robot whole-body motion transfer," in *2020 IEEE-RAS 20th International Conference on Humanoid Robots (Humanoids)*, 2021, pp. 299–305.

[46] D. Antotsiou, G. Garcia-Hernando, and T.-K. Kim,

"Task-oriented hand motion retargeting for dexterous manipulation imitation," in *Proceedings of the European Conference on Computer Vision (ECCV) Workshops*, September 2018.

[47] S. Li, X. Ma, H. Liang, M. Görner, P. Ruppel, B. Fang, F. Sun, and J. Zhang, "Vision-based teleoperation of shadow dexterous hand using end-to-end deep neural network," in *2019 International Conference on Robotics and Automation (ICRA)*, 2019, pp. 416–422.

[48] J. Liang, A. Handa, K. V. Wyk, V. Makoviychuk, O. Kroemer, and D. Fox, "In-hand object pose tracking via contact feedback and gpu-accelerated robotic simulation," in *2020 IEEE International Conference on Robotics and Automation (ICRA)*, 2020, pp. 6203–6209.

[49] A. Handa, K. Van Wyk, W. Yang, J. Liang, Y.-W. Chao, Q. Wan, S. Birchfield, N. Ratliff, and D. Fox, "Dexpilot: Vision-based teleoperation of dexterous robotic hand-arm system," in *2020 IEEE International Conference on Robotics and Automation (ICRA)*, 2020, pp. 9164–9170.

[50] Y. Qin, H. Su, and X. Wang, "From one hand to multiple hands: Imitation learning for dexterous manipulation from single-camera teleoperation," *IEEE Robotics and Automation Letters*, vol. 7, no. 4, pp. 10 873–10 881, 2022.

[51] A. Sivakumar, K. Shaw, and D. Pathak, "Robotic telekinesis: Learning a robotic hand imitator by watching humans on youtube," *Robotics: Science and Systems*, 2022. [Online]. Available: https://arxiv.org/abs/2202.10448v2

[52] Y. Qin, W. Yang, B. Huang, K. V. Wyk, H. Su, X. Wang, Y.-W. Chao, and D. Fox, "Anyteleop: A general vision-based dexterous robot arm-hand teleoperation system," *Robotics: Science and Systems*, 2023. [Online]. Available: https://arxiv.org/abs/2307.04577v3

[53] G. Brantner and O. Khatib, "Controlling ocean one: Human–robot collaboration for deep-sea manipulation," *Journal of Field Robotics*, vol. 38, no. 1, pp. 28–51, 2021. [Online]. Available: https://onlinelibrary.wiley.com/doi/abs/10.1002/rob.21960

[54] H. Li and K. Kawashima, "Bilateral teleoperation with delayed force feedback using time domain passivity controller," *Robotics and Computer-Integrated Manufacturing*, vol. 37, pp. 188–196, 2016. [Online]. Available: https://www.sciencedirect.com/science/article/pii/S0736584515000654

[55] A. Mandlekar, D. Xu, J. Wong, S. Nasiriany, C. Wang, R. Kulkarni, L. Fei-Fei, S. Savarese, Y. Zhu, and R. Mart'in-Mart'in, "What matters in learning from offline human demonstrations for robot manipulation," *Conference on Robot Learning*, 2021.

[56] H. Fang, H. Fang, Y. Wang, J. Ren, J. Chen, R. Zhang, W. Wang, and C. Lu, "Airexo: Low-cost exoskeletons for learning whole-arm manipulation in the wild," *IEEE International Conference on Robotics and Automation*, 2023. [Online]. Available: https://arxiv.org/abs/2309.14975v2

[57] K. Shaw, Y. Li, J. Yang, M. K. Srirama, R. Liu, H. Xiong, R. Mendonca, and D. Pathak, "Bimanual dexterity for complex tasks," in *8th Annual Conference on Robot Learning*, 2024. [Online]. Available: https://openreview.net/forum?id=55tYfHvanf

[58] S. Yang, M. Liu, Y. Qin, R. Ding, J. Li, X. Cheng, R. Yang, S. Yi, and X. Wang, "Ace: A cross-platform visual-exoskeletons system for low-cost dexterous teleoperation," *arXiv preprint arXiv: 2408.11805*, 2024.

[59] S. Chen, C. Wang, K. Nguyen, L. Fei-Fei, and C. K. Liu, "Arcap: Collecting high-quality human demonstrations for robot learning with augmented reality feedback," *arXiv preprint arXiv: 2410.08464*, 2024.

[60] R. S. Sutton and A. G. Barto, *Reinforcement Learning: An Introduction*, 2nd ed. The MIT Press, 2018. [Online]. Available: http://incompleteideas.net/book/the-book-2nd.html

[61] J. Ho, A. Jain, and P. Abbeel, "Denoising diffusion probabilistic models," in *Advances in Neural Information Processing Systems*, H. Larochelle, M. Ranzato, R. Hadsell, M. Balcan, and H. Lin, Eds., vol. 33. Curran Associates, Inc., 2020, pp. 6840–6851. [Online]. Available: https://proceedings.neurips.cc/paper_files/paper/2020/file/4c5bcfec8584af0d967f1ab10179ca4b-Paper.pdf

[62] A. Q. Nichol and P. Dhariwal, "Improved denoising diffusion probabilistic models," in *Proceedings of the 38th International Conference on Machine Learning*, ser. Proceedings of Machine Learning Research, M. Meila and T. Zhang, Eds., vol. 139. PMLR, 18–24 Jul 2021, pp. 8162–8171. [Online]. Available: https://proceedings.mlr.press/v139/nichol21a.html

[63] J. Sohl-Dickstein, E. Weiss, N. Maheswaranathan, and S. Ganguli, "Deep unsupervised learning using nonequilibrium thermodynamics," in *Proceedings of the 32nd International Conference on Machine Learning*, ser. Proceedings of Machine Learning Research, F. Bach and D. Blei, Eds., vol. 37. Lille, France: PMLR, 07–09 Jul 2015, pp. 2256–2265. [Online]. Available: https://proceedings.mlr.press/v37/sohl-dickstein15.html

[64] Z. Wang, J. J. Hunt, and M. Zhou, "Diffusion policies as an expressive policy class for offline reinforcement learning," *International Conference on Learning Representations*, 2022.

[65] C. Chi, Z. Xu, S. Feng, E. Cousineau, Y. Du, B. Burchfiel, R. Tedrake, and S. Song, "Diffusion policy: Visuomotor policy learning via action diffusion," *The International Journal of Robotics Research*, p. 02783649241273668, 2023. [Online]. Available: https://arxiv.org/abs/2303.04137v5

[66] Z. Wang, Z. Li, A. Mandlekar, Z. Xu, J. Fan, Y. Narang, L. Fan, Y. Zhu, Y. Balaji, M. Zhou, M.-Y. Liu, and Y. Zeng, "One-step diffusion policy: Fast visuomotor policies via diffusion distillation," *arXiv preprint arXiv: 2410.21257*, 2024. [Online]. Available:

https://arxiv.org/abs/2410.21257v1

[67] C. Qi, H. Su, K. Mo, and L. Guibas, "Pointnet: Deep learning on point sets for 3d classification and segmentation," *Computer Vision and Pattern Recognition*, 2016.

[68] O. Ronneberger, P. Fischer, and T. Brox, "U-net: Convolutional networks for biomedical image segmentation," *International Conference on Medical Image Computing and Computer-Assisted Intervention*, 2015.

[69] Y. Ze, G. Zhang, K. Zhang, C. Hu, M. Wang, and H. Xu, "3d diffusion policy: Generalizable visuomotor policy learning via simple 3d representations," *arXiv preprint arXiv: 2403.03954*, 2024. [Online]. Available: https://arxiv.org/abs/2403.03954v7

[70] X. Cheng, J. Li, S. Yang, G. Yang, and X. Wang, "Open-television: Teleoperation with immersive active visual feedback," in *8th Annual Conference on Robot Learning*, 2024. [Online]. Available: https://openreview.net/forum?id=Yce2jeILGt

[71] Y. Park and P. Agrawal, "Using apple vision pro to train and control robots," 2024. [Online]. Available: https://github.com/Improbable-AI/VisionProTeleop

[72] S. Ross, G. J. Gordon, and J. Bagnell, "A reduction of imitation learning and structured prediction to no-regret online learning," *International Conference on Artificial Intelligence and Statistics*, 2010.

[73] E. Kolve, R. Mottaghi, W. Han, E. VanderBilt, L. Weihs, A. Herrasti, M. Deitke, K. Ehsani, D. Gordon, Y. Zhu, A. Kembhavi, A. Gupta, and A. Farhadi, "Ai2-thor: An interactive 3d environment for visual ai," *arXiv preprint arXiv: 1712.05474*, 2017.

[74] X. Puig, K. Ra, M. Boben, J. Li, T. Wang, S. Fidler, and A. Torralba, "Virtualhome: Simulating household activities via programs," in *Proceedings of the IEEE Conference on Computer Vision and Pattern Recognition (CVPR)*, June 2018. [Online]. Available: https://openaccess.thecvf.com/content_cvpr_2018/html/Puig_VirtualHome_Simulating_Household_CVPR_2018_paper.html

[75] M. Shridhar, J. Thomason, D. Gordon, Y. Bisk, W. Han, R. Mottaghi, L. Zettlemoyer, and D. Fox, "Alfred: A benchmark for interpreting grounded instructions for everyday tasks," in *Proceedings of the IEEE/CVF Conference on Computer Vision and Pattern Recognition (CVPR)*, June 2020. [Online]. Available: https://openaccess.thecvf.com/content_CVPR_2020/html/Shridhar_ALFRED_A_Benchmark_for_Interpreting_Grounded_Instructions_for_Everyday_Tasks_CVPR_2020_paper.html

[76] M. Shridhar, X. Yuan, M.-A. Côté, Y. Bisk, A. Trischler, and M. J. Hausknecht, "Alfworld: Aligning text and embodied environments for interactive learning," *International Conference on Learning Representations*, 2020.

[77] J. Pari, N. M. M. Shafiullah, S. P. Arunachalam, and L. Pinto, "The surprising effectiveness of representation learning for visual imitation," *Robotics: Science and Systems*, 2021.

[78] K. Ehsani, W. Han, A. Herrasti, E. VanderBilt, L. Weihs, E. Kolve, A. Kembhavi, and R. Mottaghi, "Manipulathor: A framework for visual object manipulation," in *Proceedings of the IEEE/CVF Conference on Computer Vision and Pattern Recognition (CVPR)*, June 2021, pp. 4497–4506.

[79] L. Weihs, M. Deitke, A. Kembhavi, and R. Mottaghi, "Visual room rearrangement," in *Proceedings of the IEEE/CVF Conference on Computer Vision and Pattern Recognition (CVPR)*, June 2021, pp. 5922–5931.

[80] C. Li, F. Xia, R. Mart'in-Mart'in, M. Lingelbach, S. Srivastava, B. Shen, K. Vainio, C. Gokmen, G. Dharan, T. Jain, A. Kurenkov, K. Liu, H. Gweon, J. Wu, L. Fei-Fei, and S. Savarese, "igibson 2.0: Object-centric simulation for robot learning of everyday household tasks," *Conference on Robot Learning*, 2021.

[81] M. Bajracharya, J. Borders, D. Helmick, T. Kollar, M. Laskey, J. Leichty, J. Ma, U. Nagarajan, A. Ochiai, J. Petersen, K. Shankar, K. Stone, and Y. Takaoka, "A mobile manipulation system for one-shot teaching of complex tasks in homes," in *2020 IEEE International Conference on Robotics and Automation (ICRA)*, 2020, pp. 11 039–11 045.

[82] S. Bahl, A. Gupta, and D. Pathak, "Human-to-robot imitation in the wild," *Robotics: Science and Systems*, 2022.

[83] N. Abdo, C. Stachniss, L. Spinello, and W. Burgard, "Robot, organize my shelves! tidying up objects by predicting user preferences," in *2015 IEEE International Conference on Robotics and Automation (ICRA)*, 2015, pp. 1557–1564.

[84] C. Wang, L. J. Fan, J. Sun, R. Zhang, L. Fei-Fei, D. Xu, Y. Zhu, and A. Anandkumar, "Mimicplay: Long-horizon imitation learning by watching human play," *Conference on Robot Learning*, 2023. [Online]. Available: https://arxiv.org/abs/2302.12422v2

[85] R. Zhang, S. Lee, M. Hwang, A. Hiranaka, C. Wang, W. Ai, J. J. R. Tan, S. Gupta, Y. Hao, G. Levine, R. Gao, A. Norcia, F.-F. Li, and J. Wu, "Noir: Neural signal operated intelligent robots for everyday activities," *Conference on Robot Learning*, 2023. [Online]. Available: https://arxiv.org/abs/2311.01454v1

[86] J. Wu, R. Antonova, A. Kan, M. Lepert, A. Zeng, S. Song, J. Bohg, S. Rusinkiewicz, and T. Funkhouser, "Tidybot: personalized robot assistance with large language models," *Autonomous Robots*, vol. 47, pp. 1087–1102, 2023. [Online]. Available: https://link.springer.com/article/10.1007/s10514-023-10139-z/fulltext.html

[87] H. Shi, H. Xu, S. Clarke, Y. Li, and J. Wu, "Robocook: Long-horizon elasto-plastic object manipulation with diverse tools," *Conference on Robot Learning*, 2023. [Online]. Available: https://arxiv.org/abs/2306.14447v2

[88] A. Stone, T. Xiao, Y. Lu, K. Gopalakrishnan, K.-H. Lee, Q. Vuong, P. Wohlhart, S. Kirmani, B. Zitkovich, F. Xia, C. Finn, and K. Hausman,

"Open-world object manipulation using pre-trained vision-language models," in *7th Annual Conference on Robot Learning*, 2023. [Online]. Available: https://openreview.net/forum?id=9al6taqfTzr

[89] R. Yang, Y. Kim, A. Kembhavi, X. Wang, and K. Ehsani, "Harmonic mobile manipulation," *IEEE/RJS International Conference on Intelligent RObots and Systems*, 2023.

[90] Y. Jiang, C. Wang, R. Zhang, J. Wu, and L. Fei-Fei, "Transic: Sim-to-real policy transfer by learning from online correction," *arXiv preprint arXiv: 2405.10315*, 2024. [Online]. Available: https://arxiv.org/abs/2405.10315v3

[91] J. Yang, Z. ang Cao, C. Deng, R. Antonova, S. Song, and J. Bohg, "Equibot: Sim(3)-equivariant diffusion policy for generalizable and data efficient learning," *arXiv preprint arXiv: 2407.01479*, 2024.

[92] T. Dai, J. Wong, Y. Jiang, C. Wang, C. Gokmen, R. Zhang, J. Wu, and L. Fei-Fei, "Automated creation of digital cousins for robust policy learning," *arXiv preprint arXiv: 2410.07408*, 2024. [Online]. Available: https://arxiv.org/abs/2410.07408v3

[93] J. Wu, W. Chong, R. Holmberg, A. Prasad, Y. Gao, O. Khatib, S. Song, S. Rusinkiewicz, and J. Bohg, "Tidybot++: An open-source holonomic mobile manipulator for robot learning," *arXiv preprint arXiv: 2412.10447*, 2024. [Online]. Available: https://arxiv.org/abs/2412.10447v1

[94] K. Black, N. Brown, D. Driess, A. Esmail, M. Equi, C. Finn, N. Fusai, L. Groom, K. Hausman, B. Ichter, S. Jakubczak, T. Jones, L. Ke, S. Levine, A. Li-Bell, M. Mothukuri, S. Nair, K. Pertsch, L. X. Shi, J. Tanner, Q. Vuong, A. Walling, H. Wang, and U. Zhilinsky, "π_0: A vision-language-action flow model for general robot control," *arXiv preprint arXiv: 2410.24164*, 2024.

[95] C.-C. Hsu, B. Abbatematteo, Z. Jiang, Y. Zhu, R. Martín-Martín, and J. Biswas, "Kinscene: Model-based mobile manipulation of articulated scenes," *arXiv preprint arXiv: 2409.16473*, 2024. [Online]. Available: https://arxiv.org/abs/2409.16473v2

[96] R. Shamshiri, C. Weltzien, I. Hameed, I. Yule, T. Grift, S. Balasundram, L. Pitonakova, D. Ahmad, and G. Chowdhary, "Research and development in agricultural robotics: A perspective of digital farming," *International Journal of Agricultural and Biological Engineering*, vol. 11, pp. 1–14, 07 2018.

[97] P. Gonzalez-de Santos, R. Fernández, D. Sepúlveda, E. Navas, L. Emmi, and M. Armada, "Field robots for intelligent farms—inhering features from industry," *Agronomy*, vol. 10, no. 11, 2020. [Online]. Available: https://www.mdpi.com/2073-4395/10/11/1638

[98] S. Fountas, N. Mylonas, I. Malounas, E. Rodias, C. Hellmann Santos, and E. Pekkeriet, "Agricultural robotics for field operations," *Sensors*, vol. 20, no. 9, 2020. [Online]. Available: https://www.mdpi.com/1424-8220/20/9/2672

[99] K. G. Fue, W. M. Porter, E. M. Barnes, and G. C. Rains, "An extensive review of mobile agricultural robotics for field operations: Focus on cotton harvesting," *AgriEngineering*, vol. 2, no. 1, pp. 150–174, 2020. [Online]. Available: https://www.mdpi.com/2624-7402/2/1/10

[100] J. Delmerico, S. Mintchev, A. Giusti, B. Gromov, K. Melo, T. Horvat, C. Cadena, M. Hutter, A. Ijspeert, D. Floreano, L. M. Gambardella, R. Siegwart, and D. Scaramuzza, "The current state and future outlook of rescue robotics," *Journal of Field Robotics*, vol. 36, no. 7, pp. 1171–1191, 2019. [Online]. Available: https://onlinelibrary.wiley.com/doi/abs/10.1002/rob.21887

[101] P. Gomes, "Surgical robotics: Reviewing the past, analysing the present, imagining the future," *Robotics and Computer-Integrated Manufacturing*, vol. 27, no. 2, pp. 261–266, 2011, translational Research – Where Engineering Meets Medicine. [Online]. Available: https://www.sciencedirect.com/science/article/pii/S0736584510000608

[102] B. Peters, P. Rodrigues Armijo, C. Krause, S. Choudhury, and D. Oleynikov, "Review of emerging surgical robotic technology," *Surgical Endoscopy*, vol. 32, 04 2018.

[103] K. Cleary and C. Nguyen, "State of the art in surgical robotics: Clinical applications and technology challenges," *Computer Aided Surgery*, vol. 6, no. 6, pp. 312–328, 2001, pMID: 11954063. [Online]. Available: https://doi.org/10.3109/10929080109146301

[104] T. Z. Zhao, J. Tompson, D. Driess, P. Florence, S. K. S. Ghasemipour, C. Finn, and A. Wahid, "ALOHA unleashed: A simple recipe for robot dexterity," in *8th Annual Conference on Robot Learning*, 2024. [Online]. Available: https://openreview.net/forum?id=gvdXE7ikHI

[105] R. Ma and A. Dollar, "Yale openhand project: Optimizing open-source hand designs for ease of fabrication and adoption," *IEEE Robotics & Automation Magazine*, vol. 24, no. 1, pp. 32–40, 2017.

[106] K. Shaw, A. Agarwal, and D. Pathak, "Leap hand: Low-cost, efficient, and anthropomorphic hand for robot learning," *Robotics: Science and Systems*, 2023.

[107] K. Shaw and D. Pathak, "LEAP hand v2: Dexterous, low-cost anthropomorphic hybrid rigid soft hand for robot learning," in *2nd Workshop on Dexterous Manipulation: Design, Perception and Control (RSS)*, 2024. [Online]. Available: https://openreview.net/forum?id=eQomRzRZEP

[108] D. Gouaillier, V. Hugel, P. Blazevic, C. Kilner, J. Monceaux, P. Lafourcade, B. Marnier, J. Serre, and B. Maisonnier, "Mechatronic design of nao humanoid," in *2009 IEEE International Conference on Robotics and Automation*, 2009, pp. 769–774.

[109] J. Englsberger, A. Werner, C. Ott, B. Henze, M. A. Roa, G. Garofalo, R. Burger, A. Beyer, O. Eiberger, K. Schmid, and A. Albu-Schäffer, "Overview of

the torque-controlled humanoid robot toro," *2014 IEEE-RAS International Conference on Humanoid Robots*, pp. 916–923, 2014. [Online]. Available: https://ieeexplore.ieee.org/document/7041473

[110] P. Seiwald, S.-C. Wu, F. Sygulla, T. F. C. Berninger, N.-S. Staufenberg, M. F. Sattler, N. Neuburger, D. Rixen, and F. Tombari, "Lola v1.1 – an upgrade in hardware and software design for dynamic multi-contact locomotion," in *2020 IEEE-RAS 20th International Conference on Humanoid Robots (Humanoids)*, 2021, pp. 9–16.

[111] N. G. Tsagarakis, D. G. Caldwell, F. Negrello, W. Choi, L. Baccelliere, V. Loc, J. Noorden, L. Muratore, A. Margan, A. Cardellino, L. Natale, E. Mingo Hoffman, H. Dallali, N. Kashiri, J. Malzahn, J. Lee, P. Kryczka, D. Kanoulas, M. Garabini, M. Catalano, M. Ferrati, V. Varricchio, L. Pallottino, C. Pavan, A. Bicchi, A. Settimi, A. Rocchi, and A. Ajoudani, "Walk-man: A high-performance humanoid platform for realistic environments," *Journal of Field Robotics*, vol. 34, no. 7, pp. 1225–1259, 2017. [Online]. Available: https://onlinelibrary.wiley.com/doi/abs/10.1002/rob.21702

[112] A. SaLoutos, E. Stanger-Jones, Y. Ding, M. Chignoli, and S. Kim, "Design and development of the mit humanoid: A dynamic and robust research platform," in *2023 IEEE-RAS 22nd International Conference on Humanoid Robots (Humanoids)*, 2023, pp. 1–8.

[113] Q. Liao, B. Zhang, X. Huang, X. Huang, Z. Li, and K. Sreenath, "Berkeley humanoid: A research platform for learning-based control," *arXiv preprint arXiv: 2407.21781*, 2024. [Online]. Available: https://arxiv.org/abs/2407.21781v1

[114] H. Shi, W. Wang, S. Song, and C. K. Liu, "Toddlerbot: Open-source ml-compatible humanoid platform for loco-manipulation," *arXiv preprint arXiv: 2502.00893*, 2025.

[115] Z. Si, K. Zhang, F. Z. Temel, and O. Kroemer, "Tilde: Teleoperation for dexterous in-hand manipulation learning with a deltahand," *ROBOTICS*, 2024. [Online]. Available: https://arxiv.org/abs/2405.18804v2

[116] Y. Ishiguro, T. Makabe, Y. Nagamatsu, Y. Kojio, K. Kojima, F. Sugai, Y. Kakiuchi, K. Okada, and M. Inaba, "Bilateral humanoid teleoperation system using whole-body exoskeleton cockpit tablis," *IEEE Robotics and Automation Letters*, vol. 5, no. 4, pp. 6419–6426, 2020.

[117] A. Iyer, Z. Peng, Y. Dai, I. Guzey, S. Haldar, S. Chintala, and L. Pinto, "OPEN TEACH: A versatile teleoperation system for robotic manipulation," in *8th Annual Conference on Robot Learning*, 2024. [Online]. Available: https://openreview.net/forum?id=cvAIaS6V2I

[118] S. Song, A. Zeng, J. Lee, and T. Funkhouser, "Grasping in the wild: Learning 6dof closed-loop grasping from low-cost demonstrations," *IEEE Robotics and Automation Letters*, vol. 5, no. 3, pp. 4978–4985, 2020.

[119] S. Young, D. Gandhi, S. Tulsiani, A. Gupta, P. Abbeel, and L. Pinto, "Visual imitation made easy," in *Proceedings of the 2020 Conference on Robot Learning*, ser. Proceedings of Machine Learning Research, J. Kober, F. Ramos, and C. Tomlin, Eds., vol. 155. PMLR, 16–18 Nov 2021, pp. 1992–2005. [Online]. Available: https://proceedings.mlr.press/v155/young21a.html

[120] F. Sanches, G. Gao, N. Elangovan, R. V. Godoy, J. Chapman, K. Wang, P. Jarvis, and M. Liarokapis, "Scalable. intuitive human to robot skill transfer with wearable human machine interfaces: On complex, dexterous tasks," in *2023 IEEE/RSJ International Conference on Intelligent Robots and Systems (IROS)*, 2023, pp. 6318–6325.

[121] C. Chi, Z. Xu, C. Pan, E. A. Cousineau, B. Burchfiel, S. Feng, R. Tedrake, and S. Song, "Universal manipulation interface: In-the-wild robot teaching without in-the-wild robots," *ROBOTICS*, 2024.

[122] C. Wang, H. Shi, W. Wang, R. Zhang, F.-F. Li, and K. Liu, "Dexcap: Scalable and portable mocap data collection system for dexterous manipulation," *ROBOTICS*, 2024.

[123] M. Seo, H. A. Park, S. Yuan, Y. Zhu, and L. Sentis, "Legato: Cross-embodiment imitation using a grasping tool," *arXiv preprint arXiv: 2411.03682*, 2024.

[124] M. Shridhar, Y. L. Lo, and S. James, "Generative image as action models," *arXiv preprint arXiv: 2407.07875*, 2024. [Online]. Available: https://arxiv.org/abs/2407.07875v2

[125] N. Vahrenkamp, M. Przybylski, T. Asfour, and R. Dillmann, "Bimanual grasp planning," *2011 11th IEEE-RAS International Conference on Humanoid Robots*, pp. 493–499, 2011. [Online]. Available: https://api.semanticscholar.org/CorpusID:14784225

[126] J. Grannen, Y. Wu, B. Vu, and D. Sadigh, "Stabilize to act: Learning to coordinate for bimanual manipulation," in *7th Annual Conference on Robot Learning*, 2023. [Online]. Available: https://openreview.net/forum?id=86aMPJn6hX9F

[127] K. Harada and M. Kaneko, "Whole body manipulation," in *IEEE International Conference on Robotics, Intelligent Systems and Signal Processing, 2003. Proceedings. 2003*, vol. 1, 2003, pp. 190–195 vol.1.

[128] F. Burget, A. Hornung, and M. Bennewitz, "Whole-body motion planning for manipulation of articulated objects," in *2013 IEEE International Conference on Robotics and Automation*, 2013, pp. 1656–1662.

[129] A. Dietrich, T. Wimbock, A. Albu-Schaffer, and G. Hirzinger, "Reactive whole-body control: Dynamic mobile manipulation using a large number of actuated degrees of freedom," *IEEE Robotics & Automation Magazine*, vol. 19, no. 2, pp. 20–33, 2012.

[130] X. Xu, D. Bauer, and S. Song, "Robopanoptes: The all-seeing robot with whole-body dexterity," *arXiv preprint arXiv: 2501.05420*, 2025.

[131] F. Xia, C. Li, R. Martín-Martín, O. Litany, A. Toshev,

and S. Savarese, "Relmogen: Integrating motion generation in reinforcement learning for mobile manipulation," in *2021 IEEE International Conference on Robotics and Automation (ICRA)*, 2021, pp. 4583–4590.

[132] R. Shah, A. Yu, Y. Zhu, Y. Zhu*, and R. Martín-Martín*, "Bumble: Unifying reasoning and acting with vision-language models for building-wide mobile manipulation," *arXiv preprint*, 2024.

[133] N. Yokoyama, A. Clegg, J. Truong, E. Undersander, T.-Y. Yang, S. Arnaud, S. Ha, D. Batra, and A. Rai, "Asc: Adaptive skill coordination for robotic mobile manipulation," *IEEE Robotics and Automation Letters*, vol. 9, no. 1, pp. 779–786, 2024.

[134] Z. Fu, X. Cheng, and D. Pathak, "Deep whole-body control: Learning a unified policy for manipulation and locomotion," in *Proceedings of The 6th Conference on Robot Learning*, ser. Proceedings of Machine Learning Research, K. Liu, D. Kulic, and J. Ichnowski, Eds., vol. 205. PMLR, 14–18 Dec 2023, pp. 138–149. [Online]. Available: https://proceedings.mlr.press/v205/fu23a.html

[135] M. Liu, Z. Chen, X. Cheng, Y. Ji, R.-Z. Qiu, R. Yang, and X. Wang, "Visual whole-body control for legged loco-manipulation," *arXiv preprint arXiv: 2403.16967*, 2024. [Online]. Available: https://arxiv.org/abs/2403.16967v5

[136] H. Ha, Y. Gao, Z. Fu, J. Tan, and S. Song, "Umi on legs: Making manipulation policies mobile with manipulation-centric whole-body controllers," *arXiv preprint arXiv: 2407.10353*, 2024.

[137] X. Cheng, A. Kumar, and D. Pathak, "Legs as manipulator: Pushing quadrupedal agility beyond locomotion," in *2023 IEEE International Conference on Robotics and Automation (ICRA)*, 2023, pp. 5106–5112.

[138] Q. Wu, Z. Fu, X. Cheng, X. Wang, and C. Finn, "Helpful doggybot: Open-world object fetching using legged robots and vision-language models," in *arXiv*, 2024.

[139] P. Arm, M. Mittal, H. Kolvenbach, and M. Hutter, "Pedipulate: Enabling manipulation skills using a quadruped robot's leg," *IEEE International Conference on Robotics and Automation*, 2024. [Online]. Available: https://arxiv.org/abs/2402.10837v1

[140] X. He, C. Yuan, W. Zhou, R. Yang, D. Held, and X. Wang, "Visual manipulation with legs," in *8th Annual Conference on Robot Learning*, 2024. [Online]. Available: https://openreview.net/forum?id=E4K3yLQQ7s

[141] Y. Yamamoto and X. Yun, "Coordinating locomotion and manipulation of a mobile manipulator," in *[1992] Proceedings of the 31st IEEE Conference on Decision and Control*, 1992, pp. 2643–2648 vol.3.

[142] L. P. Kaelbling and T. Lozano-Pérez, "Integrated task and motion planning in belief space," *The International Journal of Robotics Research*, vol. 32, no. 9-10, pp. 1194–1227, 2013. [Online]. Available: https://doi.org/10.1177/0278364913484072

[143] Q. Huang, K. Tanie, and S. Sugano, "Coordinated motion planning for a mobile manipulator considering stability and manipulation," *The International Journal of Robotics Research*, vol. 19, no. 8, pp. 732–742, 2000. [Online]. Available: https://doi.org/10.1177/02783640022067139

[144] L. Sentis and O. Khatib, "A whole-body control framework for humanoids operating in human environments," in *Proceedings 2006 IEEE International Conference on Robotics and Automation, 2006. ICRA 2006.*, 2006, pp. 2641–2648.

[145] H. Dai, A. Valenzuela, and R. Tedrake, "Whole-body motion planning with centroidal dynamics and full kinematics," in *2014 IEEE-RAS International Conference on Humanoid Robots*, 2014, pp. 295–302.

[146] B. Ichter, A. Brohan, Y. Chebotar, C. Finn, K. Hausman, A. Herzog, D. Ho, J. Ibarz, A. Irpan, E. Jang, R. Julian, D. Kalashnikov, S. Levine, Y. Lu, C. Parada, K. Rao, P. Sermanet, A. Toshev, V. Vanhoucke, F. Xia, T. Xiao, P. Xu, M. Yan, N. Brown, M. Ahn, O. Cortes, N. Sievers, C. Tan, S. Xu, D. Reyes, J. Rettinghouse, J. Quiambao, P. Pastor, L. Luu, K. Lee, Y. Kuang, S. Jesmonth, N. J. Joshi, K. Jeffrey, R. J. Ruano, J. Hsu, K. Gopalakrishnan, B. David, A. Zeng, and C. K. Fu, "Do as I can, not as I say: Grounding language in robotic affordances," in *Conference on Robot Learning, CoRL 2022, 14-18 December 2022, Auckland, New Zealand*, ser. Proceedings of Machine Learning Research, K. Liu, D. Kulic, and J. Ichnowski, Eds., vol. 205. PMLR, 2022, pp. 287–318. [Online]. Available: https://proceedings.mlr.press/v205/ichter23a.html

[147] A. Brohan, N. Brown, J. Carbajal, Y. Chebotar, J. Dabis, C. Finn, K. Gopalakrishnan, K. Hausman, A. Herzog, J. Hsu, J. Ibarz, B. Ichter, A. Irpan, T. Jackson, S. Jesmonth, N. J. Joshi, R. C. Julian, D. Kalashnikov, Y. Kuang, I. Leal, K.-H. Lee, S. Levine, Y. Lu, U. Malla, D. Manjunath, I. Mordatch, O. Nachum, C. Parada, J. Peralta, E. Perez, K. Pertsch, J. Quiambao, K. Rao, M. Ryoo, G. Salazar, P. R. Sanketi, K. Sayed, J. Singh, S. Sontakke, A. Stone, C. Tan, H. Tran, V. Vanhoucke, S. Vega, Q. Vuong, F. Xia, T. Xiao, P. Xu, S. Xu, T. Yu, and B. Zitkovich, "Rt-1: Robotics transformer for real-world control at scale," *Robotics: Science and Systems*, 2022. [Online]. Available: https://arxiv.org/abs/2212.06817v2

[148] D. Honerkamp, T. Welschehold, and A. Valada, "N^2m^2: Learning navigation for arbitrary mobile manipulation motions in unseen and dynamic environments," *IEEE Transactions on robotics*, 2022.

[149] M. Xu, P. Huang, W. Yu, S. Liu, X. Zhang, Y. Niu, T. Zhang, F. Xia, J. Tan, and D. Zhao, "Creative robot tool use with large language models," *arXiv preprint arXiv: 2310.13065*, 2023.

[150] G. Pan, Q. Ben, Z. Yuan, G. Jiang, Y. Ji, S. Li,

J. Pang, H. Liu, and H. Xu, "Roboduet: Whole-body legged loco-manipulation with cross-embodiment deployment," *arXiv preprint arXiv: 2403.17367*, 2024. [Online]. Available: https://arxiv.org/abs/2403.17367v4

[151] Z. Fu, Q. Zhao, Q. Wu, G. Wetzstein, and C. Finn, "Humanplus: Humanoid shadowing and imitation from humans," *arXiv preprint arXiv: 2406.10454*, 2024. [Online]. Available: https://arxiv.org/abs/2406.10454v1

[152] C. Zhang, W. Xiao, T. He, and G. Shi, "Wococo: Learning whole-body humanoid control with sequential contacts," in *8th Annual Conference on Robot Learning*, 2024. [Online]. Available: https://openreview.net/forum?id=Czs2xH9114

[153] J. Li, Y. Zhu, Y. Xie, Z. Jiang, M. Seo, G. Pavlakos, and Y. Zhu, "OKAMI: Teaching humanoid robots manipulation skills through single video imitation," in *8th Annual Conference on Robot Learning*, 2024. [Online]. Available: https://openreview.net/forum?id=URj5TQTAXM

[154] T. He, Z. Luo, X. He, W. Xiao, C. Zhang, W. Zhang, K. M. Kitani, C. Liu, and G. Shi, "Omnih2o: Universal and dexterous human-to-humanoid whole-body teleoperation and learning," in *8th Annual Conference on Robot Learning*, 2024. [Online]. Available: https://openreview.net/forum?id=oL1WEZQal8

[155] Y. Ze, Z. Chen, W. Wang, T. Chen, X. He, Y. Yuan, X. B. Peng, and J. Wu, "Generalizable humanoid manipulation with improved 3d diffusion policies," *arXiv preprint arXiv:2410.10803*, 2024.

[156] O. M. Team, D. Ghosh, H. Walke, K. Pertsch, K. Black, O. Mees, S. Dasari, J. Hejna, T. Kreiman, C. Xu, J. Luo, Y. L. Tan, P. R. Sanketi, Q. Vuong, T. Xiao, D. Sadigh, C. Finn, and S. Levine, "Octo: An open-source generalist robot policy," *ROBOTICS*, 2024. [Online]. Available: https://arxiv.org/abs/2405.12213v2

[157] J. Yang, C. Glossop, A. Bhorkar, D. Shah, Q. Vuong, C. Finn, D. Sadigh, and S. Levine, "Pushing the limits of cross-embodiment learning for manipulation and navigation," *Robotics: Science and Systems*, 2024. [Online]. Available: https://arxiv.org/abs/2402.19432v1

[158] R. Doshi, H. R. Walke, O. Mees, S. Dasari, and S. Levine, "Scaling cross-embodied learning: One policy for manipulation, navigation, locomotion and aviation," in *8th Annual Conference on Robot Learning*, 2024. [Online]. Available: https://openreview.net/forum?id=AuJnXGq3AL

[159] A. Brohan, N. Brown, J. Carbajal, Y. Chebotar, K. Choromanski, T. Ding, D. Driess, K. A. Dubey, C. Finn, P. R. Florence, C. Fu, M. G. Arenas, K. Gopalakrishnan, K. Han, K. Hausman, A. Herzog, J. Hsu, B. Ichter, A. Irpan, N. J. Joshi, R. C. Julian, D. Kalashnikov, Y. Kuang, I. Leal, S. Levine, H. Michalewski, I. Mordatch, K. Pertsch, K. Rao, K. Reymann, M. Ryoo, G. Salazar, P. R. Sanketi, P. Sermanet, J. Singh, A. Singh, R. Soricut, H. Tran, V. Vanhoucke, Q. Vuong, A. Wahid, S. Welker, P. Wohlhart, T. Xiao, T. Yu, and B. Zitkovich, "Rt-2: Vision-language-action models transfer web knowledge to robotic control," *Conference on Robot Learning*, 2023. [Online]. Available: https://arxiv.org/abs/2307.15818v1

[160] M. J. Kim, K. Pertsch, S. Karamcheti, T. Xiao, A. Balakrishna, S. Nair, R. Rafailov, E. P. Foster, P. R. Sanketi, Q. Vuong, T. Kollar, B. Burchfiel, R. Tedrake, D. Sadigh, S. Levine, P. Liang, and C. Finn, "OpenVLA: An open-source vision-language-action model," in *8th Annual Conference on Robot Learning*, 2024. [Online]. Available: https://openreview.net/forum?id=ZMnD6QZAE6

[161] Z. Xu, H.-T. L. Chiang, Z. Fu, M. G. Jacob, T. Zhang, T.-W. E. Lee, W. Yu, C. Schenck, D. Rendleman, D. Shah, F. Xia, J. Hsu, J. Hoech, P. Florence, S. Kirmani, S. Singh, V. Sindhwani, C. Parada, C. Finn, P. Xu, S. Levine, and J. Tan, "Mobility VLA: Multimodal instruction navigation with long-context VLMs and topological graphs," in *8th Annual Conference on Robot Learning*, 2024. [Online]. Available: https://openreview.net/forum?id=JScswMfEQ0

[162] A. Mandlekar, S. Nasiriany, B. Wen, I. Akinola, Y. Narang, L. Fan, Y. Zhu, and D. Fox, "Mimicgen: A data generation system for scalable robot learning using human demonstrations," *arXiv preprint arXiv: 2310.17596*, 2023. [Online]. Available: https://arxiv.org/abs/2310.17596v1

[163] C. R. Garrett, A. Mandlekar, B. Wen, and D. Fox, "Skillmimicgen: Automated demonstration generation for efficient skill learning and deployment," in *8th Annual Conference on Robot Learning*, 2024. [Online]. Available: https://openreview.net/forum?id=YOFrRTDC6d

[164] S. Kareer, D. Patel, R. Punamiya, P. Mathur, S. Cheng, C. Wang, J. Hoffman, and D. Xu, "Egomimic: Scaling imitation learning via egocentric video," *arXiv preprint arXiv: 2410.24221*, 2024.

[165] G. Papagiannis, N. D. Palo, P. Vitiello, and E. Johns, "R+x: Retrieval and execution from everyday human videos," *arXiv preprint arXiv: 2407.12957*, 2024.

[166] K. Grauman, A. Westbury, L. Torresani, K. Kitani, J. Malik, T. Afouras, K. Ashutosh, V. Baiyya, S. Bansal, B. Boote, E. Byrne, Z. Chavis, J. Chen, F. Cheng, F.-J. Chu, S. Crane, A. Dasgupta, J. Dong, M. Escobar, C. Forigua, A. Gebreselasie, S. Haresh, J. Huang, M. M. Islam, S. Jain, R. Khirodkar, D. Kukreja, K. J. Liang, J.-W. Liu, S. Majumder, Y. Mao, M. Martin, E. Mavroudi, T. Nagarajan, F. Ragusa, S. K. Ramakrishnan, L. Seminara, A. Somayazulu, Y. Song, S. Su, Z. Xue, E. Zhang, J. Zhang, A. Castillo, C. Chen, X. Fu, R. Furuta, C. Gonzalez, P. Gupta, J. Hu, Y. Huang, Y. Huang, W. Khoo, A. Kumar, R. Kuo, S. Lakhavani, M. Liu, M. Luo, Z. Luo, B. Meredith, A. Miller, O. Oguntola, X. Pan, P. Peng, S. Pramanick,

M. Ramazanova, F. Ryan, W. Shan, K. Somasundaram, C. Song, A. Southerland, M. Tateno, H. Wang, Y. Wang, T. Yagi, M. Yan, X. Yang, Z. Yu, S. C. Zha, C. Zhao, Z. Zhao, Z. Zhu, J. Zhuo, P. Arbelaez, G. Bertasius, D. Damen, J. Engel, G. M. Farinella, A. Furnari, B. Ghanem, J. Hoffman, C. Jawahar, R. Newcombe, H. S. Park, J. M. Rehg, Y. Sato, M. Savva, J. Shi, M. Z. Shou, and M. Wray, "Ego-exo4d: Understanding skilled human activity from first- and third-person perspectives," in *Proceedings of the IEEE/CVF Conference on Computer Vision and Pattern Recognition (CVPR)*, June 2024, pp. 19 383–19 400.

[167] T. F. Gonzalez, "Clustering to minimize the maximum intercluster distance," *Theoretical Computer Science*, vol. 38, pp. 293–306, 1985. [Online]. Available: https://www.sciencedirect.com/science/article/pii/0304397585902245

[168] C. R. Qi, L. Yi, H. Su, and L. J. Guibas, "Pointnet++: Deep hierarchical feature learning on point sets in a metric space," *Advances in neural information processing systems*, vol. 30, 2017.

[169] M. Han, L. Wang, L. Xiao, H. Zhang, C. Zhang, X. Xu, and J. Zhu, "Quickfps: Architecture and algorithm co-design for farthest point sampling in large-scale point clouds," *IEEE Transactions on Computer-Aided Design of Integrated Circuits and Systems*, 2023.

[170] N. Shazeer, "Glu variants improve transformer," *arXiv preprint arXiv: 2002.05202*, 2020.

[171] K. He, X. Zhang, S. Ren, and J. Sun, "Deep residual learning for image recognition," *Computer Vision and Pattern Recognition*, 2015.

[172] I. Loshchilov and F. Hutter, "Decoupled weight decay regularization," *International Conference on Learning Representations*, 2017.

[173] J. Song, C. Meng, and S. Ermon, "Denoising diffusion implicit models," *International Conference on Learning Representations*, 2020.

APPENDIX A
ROBOT HARDWARE DETAILS

This section provides additional hardware details, including robot specifications, onboard sensors and computing, and the communication scheme.

A. Robot Hardware Specifications

1) Arms: The Galaxea R1 robot has two 6-DoF arms, each equipped with a parallel jaw gripper. As shown in Fig. A.1a, each arm has a $128\,\mathrm{mm}$ width and a $923\,\mathrm{mm}$ full reach. The arms are mirrored on the robot and are controlled via a joint impedance controller, receiving target joint positions as inputs. We set the following impedance gains: $\mathbf{K_p} = [140, 200, 120, 20, 20, 20]$ and $\mathbf{K_d} = [10, 50, 5, 1, 1, 0.4]$. Each gripper has a stroke range from $0\,\mathrm{mm}$ (fully closed) to $100\,\mathrm{mm}$ (fully open), with a rated gripping force of $100\,\mathrm{N}$. The grippers are controlled by specifying a target opening width, which is converted into the required motor current.

2) Torso: The torso consists of four revolute joints: two joints for waist rotation and hip bending, and two additional joints for knee-like motions. As shown in Fig. A.1b, the torso has a $340\,\mathrm{mm}$ width and a $1223\,\mathrm{mm}$ height (excluding the head) when fully extended. Table A.I lists the motor specifications.

TABLE A.I: **Torso motor specifications.**

Parameter	Value
Waist Joint Range (Yaw)	$\pm$ 3.05 rad (175°)
Hip Joint Range (Pitch)	$-2.09\,\mathrm{rad}$ ($-120°$) $\sim$ 1.83 rad (105°)
Knee Joint 1 Range	$-2.79\,\mathrm{rad}$ ($-160°$) $\sim$ 2.53 rad (145°)
Knee Joint 2 Range	$-1.13\,\mathrm{rad}$ ($-65°$) $\sim$ 1.83 rad (105°)
Rated Motor Torque	$108\,\mathrm{N\,m}$
Maximum Motor Torque	$304\,\mathrm{N\,m}$

3) Mobile Base: As illustrated in Fig. A.1c, the mobile base is wheeled and omnidirectional, equipped with three steering motors and three wheel motors. The base can move in any direction on the ground plane and perform yaw rotations. It is controlled via a velocity controller with 3-DoF inputs corresponding to forward velocity (x-axis), lateral velocity (y-axis), and rotation velocity (z-axis). Performance parameters are listed in Table A.II.

TABLE A.II: **Mobile base specifications.**

Parameter	Value
Forward Velocity Limit	$\pm\ 1.5\,\mathrm{m\,s^{-1}}$
Lateral Velocity Limit	$\pm\ 1.5\,\mathrm{m\,s^{-1}}$
Yaw Rotation Velocity Limit	$\pm\ 3\,\mathrm{rad\,s^{-1}}$
Forward Acceleration Limit	$\pm\ 2.5\,\mathrm{m\,s^{-2}}$
Lateral Acceleration Limit	$\pm\ 1.0\,\mathrm{m\,s^{-2}}$
Yaw Rotation Acceleration Limit	$\pm\ 1.0\,\mathrm{rad\,s^{-2}}$

B. Onboard Sensors and Computing

As shown in Fig. 3, the robot is equipped with several onboard sensors: a ZED 2 RGB-D camera (head camera), two ZED-Mini RGB-D cameras (wrist cameras), and a RealSense T265 tracking camera (visual odometry). Camera configurations are provided in Table A.III.

TABLE A.III: **Configurations for the ZED RGB-D cameras and RealSense T265 tracking camera.**

Parameter	Value
RGB-D Cameras	
Frequency	60 Hz
Image Resolution	1344×376
ZED Depth Mode	`PERFORMANCE`
Head Camera Min Depth	0.2
Head Camera Max Depth	3
Wrist Camera Min Depth	0.1
Wrist Camera Max Depth	1
Tracking Camera	
Odometry Frequency	200 Hz

The three RGB-D cameras stream colored point clouds at $60\,\mathrm{Hz}$, obtained from rectified RGB images and aligned depth images. These point clouds are fused into a common robot base frame. For each point cloud in the camera frame $\mathbf{P}^{camera}$, where $camera \in$ all cameras $= \{\text{head}, \text{left wrist}, \text{right wrist}\}$, the transformation from the robot base frame to camera frames is computed using forward kinematics at $500\,\mathrm{Hz}$. Denote rotation matrices as $\mathbf{R}^{camera} \in \mathbb{R}^{3\times3}$ and translations as $\mathbf{t}^{camera} \in \mathbb{R}^{3\times1}$, the fused, ego-centric point cloud $\mathbf{P}^{\text{ego-centric}}$ is computed as:

$$\mathbf{P}^{\text{ego-centric}} = \bigcup_{camera}^{\text{all cameras}} \mathbf{P}^{camera} \left(\mathbf{R}^{camera}\right)^{\intercal} + \left(\mathbf{t}^{camera}\right)^{\intercal}. \tag{A.1}$$

An example of the fused ego-centric colored point cloud is shown in Fig. A.2. The point cloud is then spatially cropped and downsampled using farthest point sampling (FPS) [167–169].

The RealSense T265 tracking camera provides 6D velocity and acceleration feedback at $200\,\mathrm{Hz}$. It is mounted on the back of the mobile base using a custom-designed camera mount.

The R1 robot is equipped with an NVIDIA Jetson Orin, dedicated to running cameras and processing observations at a high rate.

C. Communication Scheme

The robot communicates with a workstation via the Robot Operating System (ROS). Each camera operates as an individual ROS node. The workstation runs the master ROS node, which subscribes to robot state nodes and camera nodes, and issues control commands via ROS topics. To reduce latency, a local area network (LAN) is established between the workstation and the robot.

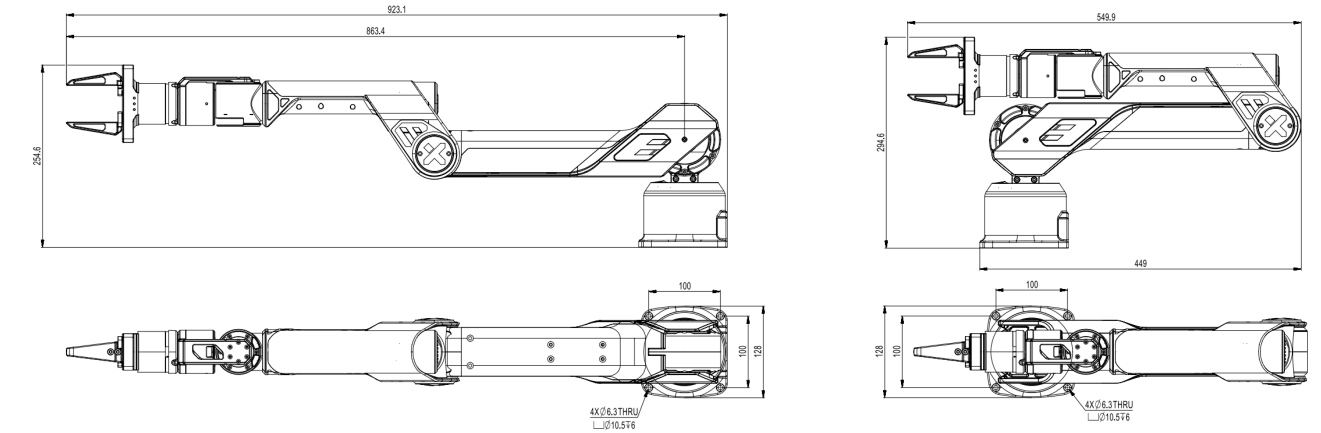

(a)

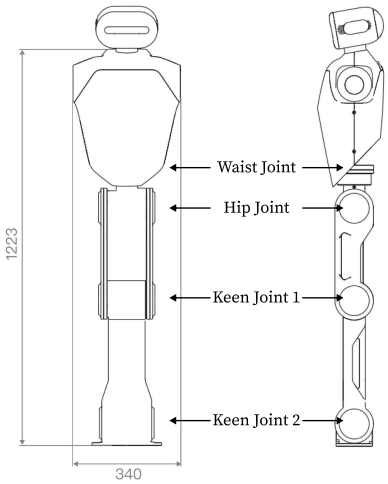

(b)

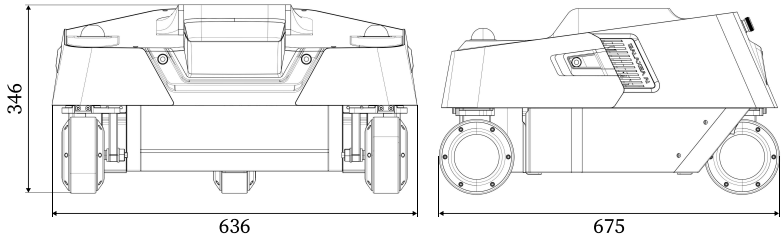

(c)

Fig. A.1: **Robot diagrams. (a):** Each arm has six DoFs and a parallel jaw gripper. **(b):** The torso features four revolute joints for waist rotation, hip bending, and knee-like motions. **(c):** The wheeled, omnidirectional mobile base is equipped with three steering motors and three wheel motors.

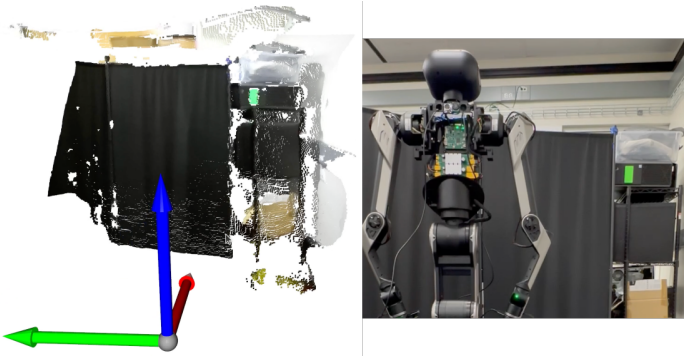

Fig. A.2: **Visualization of the fused, ego-centric colored point clouds. Left:** The colored point cloud observation, aligned with the robot's coordinate frame. **Right:** The robot's orientation and its surrounding environment.

APPENDIX B
JOYLO DETAILS

This section provides details on JoyLo, including its hardware components, controller implementation, and data collection process.

A. Hardware Components

The JoyLo system consists of 3D-printable arm links, low-cost Dynamixel motors, and off-the-shelf Joy-Con controllers. The individual arm links are shown in Fig. A.3. Using a Bambu Lab P1S 3D printer, we printed two arms in 13 h, consuming 317 g of PLA filament. The bill of materials is listed in Table A.IV. Once assembled, we use the official Dynamixel SDK to read motor states at 400 Hz - 500 Hz. The Joy-Cons connect to the workstation via Bluetooth, communicating at 66 Hz.

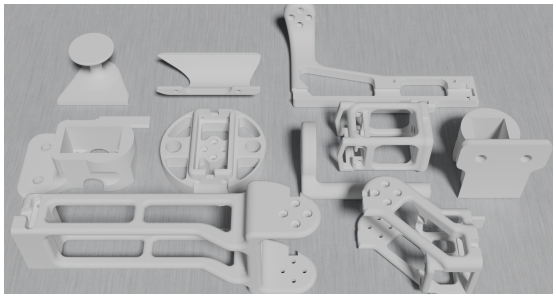

Fig. A.3: **Individual JoyLo arm links.**

B. Controller Implementation

We provide an intuitive, real-time Python-based controller to operate JoyLo with the R1 robot. As illustrated in Pseudocode 1, the controller includes a joint impedance controller for the torso and arms with target joint positions as inputs, and a velocity controller for the mobile base with target base velocities as inputs. Control commands are converted into waypoints and sent to the robot via ROS topics at 100 Hz, which we find to be sufficient in practice.

```
from bctrl.robot_interface import R1Interface

# instantiate the controller
robot = R1Interface(...)
# send a control command
robot.control(
    # the torso and arms commands are target joint
    positions
    arm_cmd={
        "left": left_arm_target_q,
        "right": right_arm_target_q,
    },
    gripper_cmd={
        "left": left_gripper_target_width,
        "right": left_gripper_target_width,
    },
    torso_cmd=torso_target_q,
    # the mobile base commands are target velocities
    base_cmd=mobile_base_target_velocity,
)
```

Pseudocode 1: **Python interface for the R1 robot controller.**

To enable bilateral teleoperation of JoyLo arms as discussed in Sec. II-B, we implement a joint impedance controller using current-based control, computed as Eq. 1, where force is proportional to motor current. We set proportional gains $\mathbf{K_p} = [0.5, 1.2, 1.2, 1.2, 1.2, 1.2]$ and derivative gains $\mathbf{K_d} = [0.01, 0.01, 0.01, 0.01, 0.01, 0.01]$.

C. Data Collection

During data collection, the robot operates at 100 Hz, while samples are recorded at 10 Hz. Functional buttons on the right Joy-Con (Fig. 3) control start, pause, save, and discard actions. Recorded data includes RGB images, depth images, point clouds, joint states, odometry, and action commands.

APPENDIX C
MODEL ARCHITECTURES, POLICY TRAINING, AND DEPLOYMENT DETAILS

This section provides details on WB-VIMA and baseline model architectures, policy training, and real-robot deployment.

A. WB-VIMA Architecture

1) Observation Encoder: As introduced in Sec. III-B, there are two types of observation tokens: the point-cloud token $\mathbf{E}^{\text{pcd}}$ and the proprioceptive token $\mathbf{E}^{\text{prop}}$. A colored point-cloud observation is denoted as $\mathbf{P}^{\text{colored pcd}} \in \mathbb{R}^{N_{\text{pcd}} \times 6}$, where N_{pcd} is the number of points in the point cloud. Each point contains six channels: three for RGB values and three for spatial coordinates. To encode point-cloud tokens, RGB values are normalized to $[0, 1]$ by dividing by 255; spatial coordinates are normalized to $[-1, 1]$ by dividing by task-specific spatial limits; finally A PointNet encoder [67] processes the point cloud. Proprioceptive observations include the mobile base velocity $v_{\text{mobile base}} \in \mathbb{R}^3$, torso joint positions $q_{\text{torso}} \in \mathbb{R}^4$, arms joint positions $q_{\text{arms}} \in \mathbb{R}^{12}$, and gripper widths $q_{\text{grippers}} \in \mathbb{R}^2$. These values are concatenated and processed through an MLP. Model hyperparameters for the PointNet and proprioception MLP are listed in Table A.V.

2) Multi-Modal Observation Attention: To effectively fuse multi-modal observations, WB-VIMA employs a multi-modal observation attention network—a transformer decoder that applies causal self-attention over the input sequence: $\mathbf{S} = [\mathbf{E}^{\text{pcd}}_{t-T_o+1}, \mathbf{E}^{\text{prop}}_{t-T_o+1}, \mathbf{E}^{\text{a}}_{t-T_o+1}, \ldots, \mathbf{E}^{\text{pcd}}_{t}, \mathbf{E}^{\text{prop}}_{t}, \mathbf{E}^{\text{a}}_{t}] \in \mathbb{R}^{3T_o \times E}$, where T_o is the observation window size, E is the token dimension, and $\mathbf{E}^{\text{a}}$ represents the action readout token. The transformer decoder's hyperparameters are listed in Table A.VI. Action readout tokens are passive and do not influence the transformer output; they only attend to previous observation tokens to maintain causality. The final action readout token at time step t, $\mathbf{E}^{a}_{t}$, is used for autoregressive whole-body action decoding. We use an observation window size of $T_o = 2$ for all methods.

3) Autoregressive Whole-Body Action Denoising: As discussed in Sec. III-B, WB-VIMA jointly learns three independent denoising networks for the mobile base, torso, and arms, denoted as ϵ_{base}, ϵ_{torso}, and ϵ_{arms}, respectively. Each

TABLE A.IV: **JoyLo bill of materials.**

Item No.	Part Name	Description	Quantity	Unit Price ($)	Total Price ($)	Supplier
1	Dynamixel XL330-M288-T	JoyLo arm joint motors	16	23.90	382.40	Dynamixel
2	Nintendo Joy-Con	JoyLo hand-held controllers	1	70	70	Nintendo
3	Dynamixel U2D2	USB communication converter for controlling Dynamixel motors	1	32.10	32.10	Dynamixel
4	5V DC Power Supply	Power supply for Dynamixel motors	1	<10	<10	Various
5	3D Printer PLA Filament	PLA filament for 3D printing JoyLo arm links	1	∼5	∼5	Various

Total Cost: ∼$499.5

TABLE A.V: **Hyperparameters for PointNet and the proprioception MLP.**

Hyperparameter	Value	Hyperparameter	Value
PointNet		Prop. MLP	
N_{pcd}	4096	Input Dim	21
Hidden Dim	256	Hidden Dim	256
Hidden Depth	2	Hidden Depth	3
Output Dim	256	Output Dim	256
Activation	GELU	Activation	ReLU

TABLE A.VI: **Hyperparameters for the transformer decoder used in multi-modal observation attention.**

Hyperparameter	Value
Embed Size	256
Num Layers	2
Num Heads	8
Dropout Rate	0.1
Activation	GEGLU [170]

denoising network is implemented using a UNet [68], with hyperparameters listed in Table A.VII. The denoising process follows three sequential steps. First, the mobile base denoising network ϵ_{base} takes the action readout token $\mathbf{E}^a$ as input and predicts future mobile base actions $\mathbf{a}_{\text{base}} \in \mathbb{R}^{T_a \times 3}$. Subsequently, the torso denoising network ϵ_{torso} takes $\mathbf{E}^a$ and $\mathbf{a}_{\text{base}}$ as input and predicts future torso actions $\mathbf{a}_{\text{torso}} \in \mathbb{R}^{T_a \times 4}$. Finally, the arms denoising network ϵ_{arms} takes $\mathbf{E}^a$, $\mathbf{a}_{\text{base}}$, and $\mathbf{a}_{\text{torso}}$ as input and predicts future arm and gripper actions $\mathbf{a}_{\text{arms}} \in \mathbb{R}^{T_a \times 14}$. Here T_a is the action prediction horizon, and we use $T_a = 8$ hereafter. To ensure low-latency inference, denoising starts from the encoded action readout tokens, meaning the observation encoders and transformer run only once per inference call.

TABLE A.VII: **Hyperparameters for the UNet models used for denoising.**

Hyperparameter	Value
Hidden Dim	[64,128]
Kernel Size	2
GroupNorm Num Groups	5
Diffusion Step Embd Dim	8

B. Baselines Architectures

We provide details on baseline methods DP3 [69] and RGB-DP [65]. DP3 uses the same PointNet encoder as WB-VIMA (Table A.V), but ignores RGB channels. Proprioceptive features are processed through the same MLP encoder. Encoded features are concatenated and passed through a fusion MLP with two hidden layers and 512 hidden units. A UNet denoising network (Table A.VII) predicts a flattened 21-DoF whole-body action trajectory. RGB-DP is similar to DP3 but uses a pre-trained ResNet-18 [171] as the vision encoder. The last classification layer is replaced with a 512-dimensional output layer for policy learning.

C. Policy Training Details

Policies are trained using the AdamW optimizer [172], with hyperparameters in Table A.VIII. 90% of collected data is used for training, and 10% is reserved for validation. Policies are trained for equal steps, using the last checkpoint for evaluation. During training, we use the DDPM noise scheduler [61–63] with 100 denoising steps. During evaluation and inference, we use the DDIM noise scheduler [173] with 16 denoising steps. Training is performed using Distributed Data Parallel (DDP) on NVIDIA GPUs, including RTX A5000, RTX 4090, and A40.

TABLE A.VIII: **Training hyperparameters.**

Hyperparameter	Value
Learning Rate	7×10^{-4}
Weight Decay	0.1
Learning Rate Warm Up Steps	1000
Learning Rate Cosine Decay Steps	300,000
Minimal Learning Rate	5×10^{-6}

D. Policies Deployment Details

During deployment, observations from the robot's onboard sensors are transmitted to a workstation, where policy inference is performed, and the resulting actions are sent back for execution. To minimize latency, we implement asynchronous policy inference. Concretely, policy inference runs continuously in the background. When switching to a new predicted trajectory, the initial few actions are discarded to compensate for inference latency. This ensures non-blocking execution, preventing delays caused by observation acquisition and controller execution.

APPENDIX D
TASK DEFINITION AND EVALUATION DETAILS

This section provides detailed task definitions, generalization conditions, and evaluation protocols.

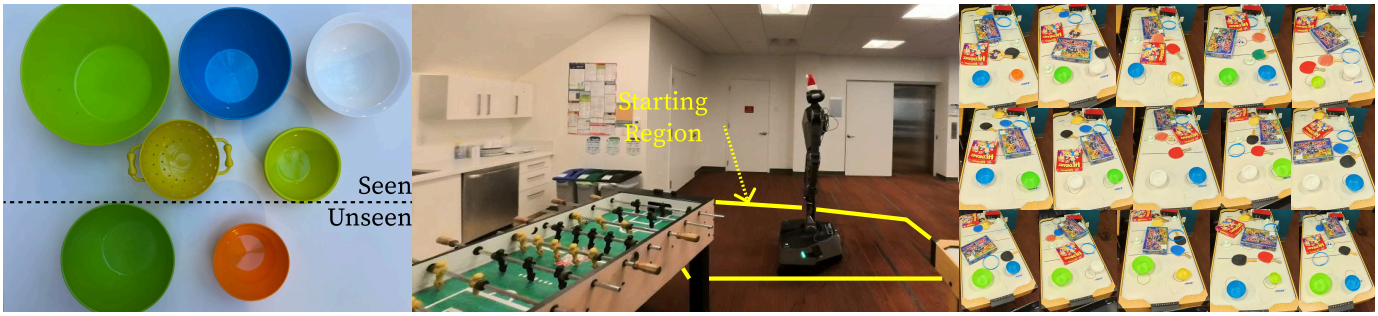

Fig. A.4: **Generalization settings for the task "clean house after a wild party".** From left to right: seen and unseen bowl variations, robot's starting region, and initial object placements on the gaming table.

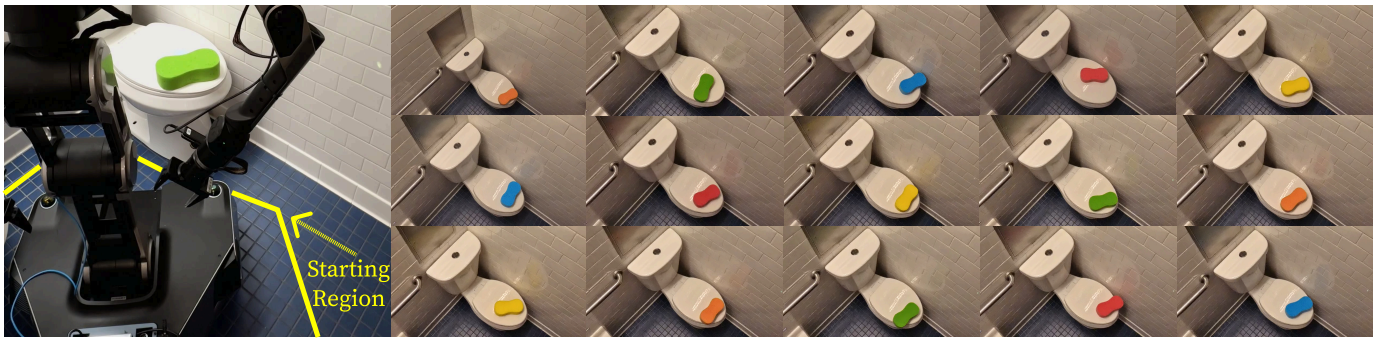

Fig. A.5: **Generalization settings for the task "clean the toilet".** From left to right: robot's starting region, sponge variations, and initial placements.

A. Task Definition

Activity 1 ***Clean House After a Wild Party*** *(Fig. 1 First Row)*: Starting in the living room, the robot navigates to a dishwasher in the kitchen (**ST-1**) and opens it (**ST-2**). It then moves to a gaming table (**ST-3**) to collect bowls (**ST-4**). Finally, the robot returns to the dishwasher (**ST-5**), places the bowls inside, and closes it (**ST-6**). Stable and accurate navigation is the most critical capability for this task. We collect 138 demonstrations, with an average human completion time of 210 s. As shown in Fig. A.4, we randomize the starting position of the robot, bowl instances and their placements, and distractors on the table.

Activity 2 ***Clean the Toilet*** *(Fig. 1 Second Row)*: In a restroom, the robot picks up a sponge placed on a closed toilet (**ST-1**), opens the toilet cover (**ST-2**), cleans the seat (**ST-3**), closes the cover (**ST-4**), and wipes it (**ST-5**). The robot then moves to press the flush button (**ST-6**). Extensive end-effector reachability is the most critical capability for this task. We collect 103 demonstrations, with an average human completion time of 120 s. As shown in Fig. A.5, we randomize the robot starting position, sponge instances, and placements.

Activity 3 ***Take Trash Outside*** *(Fig. 1 Third Row)*: The robot navigates to a trash bag in the living room, picks it up (**ST-1**), carries it to a closed door (**ST-2**), opens the door (**ST-3**), moves outside, and deposits the trash bag into a trash bin (**ST-4**). Stable and accurate navigation is the most critical capability for this task. We collect 122 demonstrations, with an average human completion time of 130 s. As shown in Fig. A.6, we randomize the robot starting position and the placement of the trash bag.

Fig. A.6: **Generalization settings for the task "take trash outside".** From left to right: initial placement region of the trash bag and robot's starting region.

Activity 4 ***Put Items onto Shelves*** *(Fig. 1 Fourth Row)*: In a storage room, the robot lifts a box from the ground (**ST-1**), moves to a four-level shelf, and places the box on the appropriate level based on available space (**ST-2**). Extensive end-effector reachability is the most critical capability for this task. We collect 100 demonstrations, with an average human completion time of 60 s. As shown in Fig. A.7, we randomize the robot starting position, box placement, objects inside the box, shelf empty spaces, and distractors.

Activity 5 ***Lay Clothes Out*** *(Fig. 1 Fifth Row)*: In a bedroom, the robot moves to a wardrobe, opens it (**ST-1**), picks up a jacket on a hanger (**ST-2**), lays the jacket on a sofa bed (**ST-3**), and then returns to close the wardrobe (**ST-4**). Bimanual

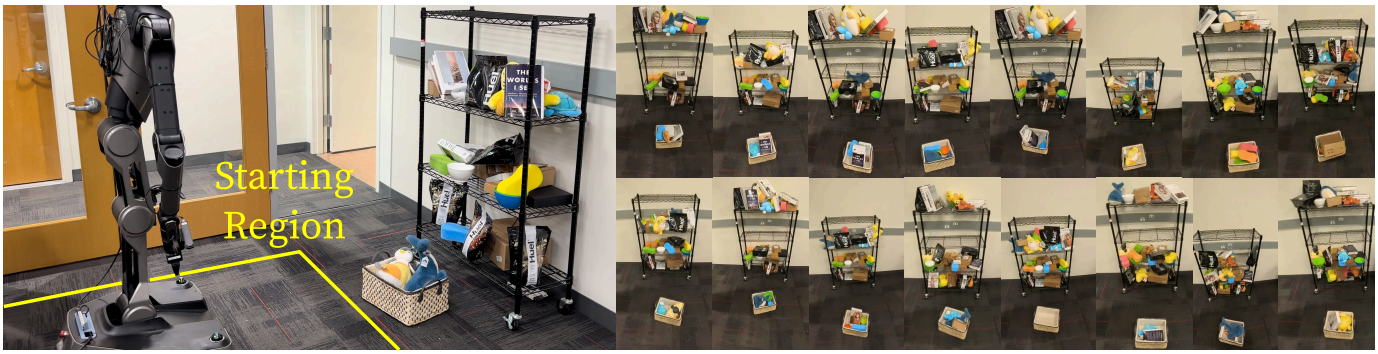

Fig. A.7: **Generalization settings for the task "put items onto shelves".** From left to right: robot's starting region, box placements, and shelf configurations.

Fig. A.8: **Generalization settings for the task "lay clothes out".** From left to right: robot's starting region, clothing placements, and clothing variations.

coordination is the most critical capability for this task. We collect 98 demonstrations, with an average human completion time of 120 s. As shown in Fig. A.8, we randomize the robot starting position, clothing placements, and clothing instances.

B. Policy Evaluation Results

Numerical results from policy evaluation are presented in Tables A.IX, A.X, A.XI, A.XII, and A.XIII.

C. User Study Details

As described in Sec. IV-C, we conducted a user study with 10 participants to compare JoyLo against two alternative interfaces: VR controllers [25] and Apple Vision Pro [70, 71]. The study was conducted in the OmniGibson simulator [8] on the task "clean house after a wild party". To provide equal depth perception, participants wore a Meta Quest 3 headset while using both JoyLo and VR controllers. To eliminate bias, participants were exposed to the three interfaces in a randomized order. Each participant had a 10-minute practice session for each interface before beginning the formal evaluation. A successful task rollout is shown in Fig. A.9.

After the sessions, rollouts were manually segmented, and task and sub-task completions were annotated using a GUI (Fig. A.10). For VR controllers and Apple Vision Pro, which use inverse kinematics (IK) based on end-effector poses, singular configurations were identified when the Jacobian matrix's condition number exceeded a set threshold. For JoyLo, which directly controls joints, excessive joint velocities were used as an indicator of singular or near-singular configurations. The post-session survey questions sent to participants are listed below:

- $\mathcal{Q}\mathbf{1}$: Do you have prior data collection experience in robot learning? [Yes/No]
- $\mathcal{Q}\mathbf{2}$: Before the session, which device did you expect to be the most user-friendly? [VR Controllers/Apple Vision Pro/JoyLo]
- $\mathcal{Q}\mathbf{3}$: After the session, which device did you find to be the most user-friendly? [VR Controllers/Apple Vision Pro/JoyLo]
- $\mathcal{Q}\mathbf{4}$: Did physically holding JoyLo arms help with data collection? [Yes/No]
- $\mathcal{Q}\mathbf{5}$: Did using thumbsticks for torso and mobile base move-

Fig. A.9: **Successful task completion by a participant.** The robot navigates to a dishwasher and opens it, moves to a table to collect teacups, returns to the dishwasher, places the teacups inside, and closes it.

ment improve control? [Yes/No]

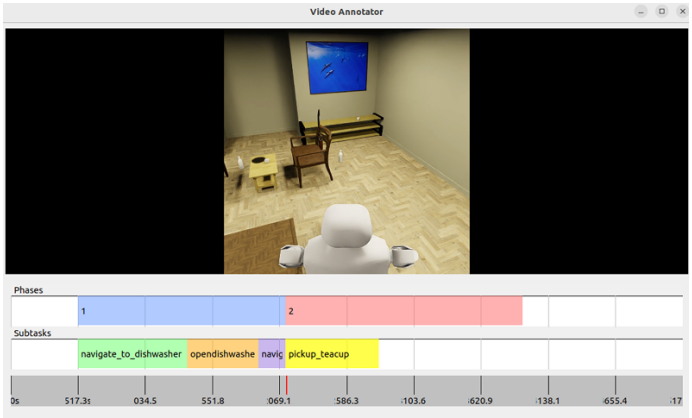

Fig. A.10: **GUI for annotating user study rollouts.**

TABLE A.IX: **Numerical evaluation results for the task "clean house after a wild party".** Success rates are shown as percentages. Values in parentheses indicate the number of successful trials out of the total trials.

	ET	ST-1	ST-2	ST-3	ST-4	ST-5	ST-6	Safety Violations
Human	68% (50/73)	100% (73/73)	93% (69/74)	100% (69/69)	89% (64/72)	94% (60/64)	88% (53/60)	N/A
Ours	**40% (6/15)**	**100% (15/15)**	**80% (12/15)**	**80% (12/15)**	**73% (11/15)**	**93% (14/15)**	**93% (14/15)**	**0**
DP3 [69]	0% (0/15)	80% (12/15)	7% (1/15)	27% (4 / 15)	7% (1/15)	33% (5/15)	40% (6/15)	13
RGB-DP [65]	0% (0/15)	93% (14/15)	0% (0/15)	0% (0/15)	7% (1/15)	7% (1/15)	20% (3/15)	2

TABLE A.X: **Numerical evaluation results for the task "clean the toilet".** Success rates are shown as percentages. Values in parentheses indicate the number of successful trials out of the total trials.

	ET	ST-1	ST-2	ST-3	ST-4	ST-5	ST-6	Safety Violations
Human	61% (100/164)	91% (150/164)	72% (106/148)	99% (104/105)	100% (103/103)	98% (102/104)	98% (100/102)	N/A
Ours	**53% (8/15)**	**100% (15/15)**	**80% (12/15)**	**100% (15/15)**	**100% (15/15)**	**100% (15/15)**	**73% (11/15)**	**0**
DP3 [69]	0% (0/15)	**100% (15/15)**	47% (7/15)	93% (14/15)	0% (0/15)	13% (2/15)	0% (0/15)	**0**
RGB-DP [65]	0% (0/15)	93% (14/15)	13% (2/15)	7% (1/15)	7% (1/15)	0% (0/15)	20% (3/15)	2

TABLE A.XI: **Numerical evaluation results for the task "take trash outside".** Success rates are shown as percentages. Values in parentheses indicate the number of successful trials out of the total trials.

	ET	ST-1	ST-2	ST-3	ST-4	Safety Violations
Human	76% (96/127)	91% (116/128)	100% (124/124)	85% (106/125)	100% (115/115)	N/A
Ours	**53% (8/15)**	**80% (12/15)**	**100% (15/15)**	**87% (13/15)**	**87% (13/15)**	**1**
DP3 [69]	0% (0/15)	60% (9/15)	53% (8/15)	20% (3/15)	7% (1/15)	9
RGB-DP [65]	0% (0/15)	20% (3/15)	7% (1/15)	7% (1/15)	7% (1/15)	3

TABLE A.XII: **Numerical evaluation results for the task "put items onto shelf".** Success rates are shown as percentages. Values in parentheses indicate the number of successful trials out of the total trials.

	ET	ST-1	ST-2	Safety Violations
Human	89% (93/104)	90% (94/104)	100% (93/93)	N/A
Ours	**93% (14/15)**	**93% (14/15)**	**100% (15/15)**	**0**
DP3 [69]	20% (3/15)	27% (4/15)	47% (7/15)	**0**
RGB-DP [65]	13% (2/15)	20% (3/15)	40% (6/15)	**0**
Ours w/o W.B. Action Denoising	40% (6/15)	40% (6/15)	60% (9/15)	**0**
Ours w/o Multi-Modal Obs. Attn.	13% (2/15)	33% (5/15)	40% (6/15)	**0**

TABLE A.XIII: **Numerical evaluation results for the task "lay clothes out".** Success rates are shown as percentages. Values in parentheses indicate the number of successful trials out of the total trials.

	ET	**ST-1**	**ST-2**	**ST-3**	**ST-4**	**Safety Violations**
Human	50% (54/108)	56% (60/108)	93% (56/60)	96% (54/56)	100% (54/54)	N/A
Ours	**53% (8/15)**	**87% (13/15)**	**93% (14/15)**	**80% (12/15)**	60% (9/15)	**0**
DP3 [69]	0% (0/15)	13% (2/15)	13% (2/15)	27% (4/15)	27% (4/15)	7
RGB-DP [65]	0% (0/8)	13% (1/8)	25% (2/8)	13% (1/8)	13% (1/8)	3
Ours w/o W.B. Action Denoising	13% (2/15)	33% (5/15)	73% (11/15)	73% (11/15)	**67% (10/15)**	**0**
Ours w/o Multi-Modal Obs. Attn.	0% (0/15)	33% (5/15)	40% (6/15)	47% (7/15)	13% (2/15)	4